Hindawi
International Journal of Chemical Engineering
Volume 2022, Article ID 6928568, 24 pages
https://doi.org/10.1155/2022/6928568

Research Article

Kinetics and Equilibrium Studies of the Adsorption of Copper(II) Ions from Industrial Wastewater Using Activated Carbons Derived from Sugarcane Bagasse

Temiloluwa E. Amoo,[1] **Kehinde O. Amoo**,[1,2] **Opeyemi A. Adeeyo**,[1] **and Clement O. Ogidi**[3]

[1]*Department of Chemical Engineering, Covenant University, Km 10, Idiroko Road, Canaan Land, Ota, Nigeria*
[2]*Department of Chemical and Polymer Engineering, Lagos State University, Lagos, Nigeria*
[3]*Department of Food Science and Technology, School of Agriculture, Food and Natural Resources, Olusegun Agagu University of Science and Technology, PMB 353, Okitipupa, Nigeria*

Correspondence should be addressed to Kehinde O. Amoo; kehinde.amoo@yahoo.com

Received 15 December 2021; Revised 7 March 2022; Accepted 23 March 2022; Published 23 April 2022

Academic Editor: Maurizio Volpe

Copyright © 2022 Temiloluwa E. Amoo et al. This is an open access article distributed under the Creative Commons Attribution License, which permits unrestricted use, distribution, and reproduction in any medium, provided the original work is properly cited.

The monocomponent adsorption process of Cu(II) ions in synthesized industrial wastewater were investigated using activated carbons (BACs) derived from sugarcane bagasse as the precursor. Batch adsorption studies were done by treating the precursor with H_3PO_4 (BAC-P) and $ZnCl_2$ (BAC-Zn) in order to observe the effects of experimental variables such as contact time, pH of the solution, and adsorbent dose. The Langmuir isotherm model excellently described the adsorption data for both the derived BACs, indicating monolayer coverage on the BACs with the determination coefficients close to the value of one. Furthermore, the maximum adsorption capacities of 589 and 225 $mg\,g^{-1}$ at 30°C were obtained for BAC-P and BAC-Zn adsorbents, respectively. The modeling of kinetic data of Cu(II) ions adsorption onto BAC-P and BAC-Zn adsorbents illustrated that the Elovich kinetic model fitted well. Here, the adsorption process was film-diffusion controlling, while being principally governed by external mass transport where the slowest step is the diffusion of the particles through the film layer. The mechanism of the adsorption process was proposed taking into cognizance of the ion exchange and surface complexation on active sites between the negatively charged surface of the BACs and the positively charged Cu(II) ions. The BACs were characterized using analytical methods such as SEM, FTIR, EDX, XRD, BET surface area, and zeta potential measurements. Both BACs mainly composed of mesopores and bonds of O-H, C-O, C=O, and C-O-C. The BET surface area of BAC-P and BAC-Zn was 427.5 and 282 m^2/g before adsorption, and their isoelectric point (pH_{IEP}) 3.70 and 5.26, respectively.

1. Introduction

Waste production cannot be isolated from the existence of humanity. The quantity of waste generated is associated with the increase in population. Versilind et al. [1] came up with the fact that waste is a consequence of the daily activities of all creatures. Today, evidence gathered from data concludes that the future of planet Earth is at stake, and the coming generations will suffer if humans continue to destroy the environment at this current rate [2]. The side effects of improper or poor management of wastes are usually manifested in the environment by causing distress on human health and also having negative impacts on the economy [3].

The economic importance of sugarcane (*Saccharum sinense*) cannot be overemphasized. This is because sugarcane is one of the most consumed crops with high cellulose content [4]. Sugarcane is put into many uses worldwide such as a source of bioethanol, sugar, heat, and paper manufacture [5, 6].

The Food and Agriculture Organization (FAO) in 2017 [7] released a report that the cultivation of sugarcane on about 26 million hectares of land in more than 90 countries

worldwide resulted in a harvest of 1.83 billion ton/year. Statistics show that 80% of sugar is produced from sugarcane [4]; most of the rest is made from sugar beet. It has been revealed that for every 1 ton of sugar, 0.3 ton of bagasse is produced [8], making sugarcane bagasse one of the most generated solid wastes in the world.

Sugarcane bagasse—an undesirable by-product of the sugar manufacturing industry and domestic consumption—is one of the most generated solid wastes in the world based on sugarcane cultivation, demand, and usage statistics; it has been significantly underutilized. The choice of sugarcane bagasse and its derivatives as adsorbents in adsorption processes has not been thoroughly investigated. Sugarcane bagasse and its derivatives when used as adsorbents could be economical, sustaining, and alternative materials to other uses. Sugarcane bagasse can be synthesized into activated carbon; a beneficial, effective, and efficient material in the treatment of industrial wastewater. Faur-Brasquet et al. [9] revealed in their investigation that activated carbon, in general, serves as a very effective agent for the removal of heavy metals (copper, calcium, magnesium, nickel, etc.) from industrial wastewater due to its unique sorption characteristics.

The significant consequence of improper waste management systems is pollution to freshwater and saltwater bodies. This is usually caused by the release of untreated industrial waste into the environment and water bodies. There have been projections that 20 million hectares of cultivatable land is irrigated with wastewater of some kind [10]. These industrial wastewaters from mining, metal processing, and petroleum industries contain harmful chemical substances such as heavy metals, which include copper, chromium, nickel, lead, mercury, etc., that are harmful to the environment and humans. Copper specifically is a highly toxic heavy metal and is poisonous to all living organisms when accumulated over an extended period [11]. It is also known to have carcinogenic effects on humans, and this poses a great threat to human health and security [11–13]. Although Cu(II) ions are an essential element for good growth and healthy bodily functions in living organisms [14], prolonged ingestion of copper is known to cause damage to cells, which may lead to Wilson's disease in human beings [11]. The greatest cause for concern with respect to copper poisoning is the corrosion of pipes, thereby increasing the possibility of Cu^{2+} entering into homes' faucets and taps [15], which is really difficult to detect even at relatively high concentrations.

There have been several attempts and methods that have been employed in removing heavy metals from wastewater [16]; methods such as liquid-liquid extraction [17], membrane filtration [18], chemical coagulation [19], phytoremediation [20, 21], and ion exchange [22] are highly sensitive, not particularly effective, require costly equipment and instrumentation, laboratory system setup, complex procedural requirements, highly skilled personnel, and an immense recurrent expenditure and operating cost [14]. These drawbacks make these methods unsuitable for long-term continuous use or on-site or field investigation [23].

In recent years, though, more effective and economical technologies have been adopted to reduce the contaminants in and improve the quality of industrial wastewaters [24]. Liquid-phase adsorption has been one of the most important of these technologies due to its low cost and effectiveness [25, 26]. The effectiveness of the adsorbent is measured by its ability to meet the maximum contaminant level (MCL) standards established as issued by the United States Environmental Protection Agency (USEPA) [27, 28]. The availability and low cost of sugarcane bagasse established it as a renewable resource, a material that can be successfully used for many adsorption processes, and as a precursor for activated carbon [29, 30].

Therefore, this research work aims at investigating the monocomponent adsorption behaviour of copper(II) ions onto activated carbons derived from sugarcane bagasse (BACs). A very compelling reason as to why copper metal ions were selected for this study is that, not only is it on the 126 Priority Pollutant List (120) as regulated by the United States Environmental Protection Agency (USEPA), copper ions are really dangerous to the human health [28] even at low concentrations. From the above framework, the specific objective of the adsorption process was to prepare activated carbon from dried sugarcane bagasse using phosphoric acid (H_3PO_4) and zinc chloride ($ZnCl_2$) as chemical activating agents to form phosphoric acid activated carbon (BAC-P) and zinc chloride activated carbon (BAC-Zn), respectively. Furthermore, to determine the mechanisms governing the adsorption process of Cu(II) ions removal from simulated wastewater, different adsorption isotherms (Langmuir, Freundlich, Elovich, and Sips) and kinetic models (pseudo-first-order, pseudo-second-order, intraparticle diffusion, and Boyd) were correlated with experimental data to obtain the best fits describing the adsorbent-adsorbate interactions.

2. Materials and Methods

2.1. Chemicals and Reagents. Phosphoric acid (85%) and hydrochloric acid (85%) were purchased from Sigma-Aldrich Co. (Merck, Darmstadt, Germany). Zinc chloride crystals (98%) and sodium hydroxide pellets (97%) were purchased from J.T. Baker Co. (Phillipsburg, USA). Deionized water was generated using a Labtech ultrapure water deionizer. The stock solutions of copper(II) ions were prepared using $CuSO_4.5H_2O$ purchased from J.T. Baker Co. (Phillipsburg, USA). All the chemicals that were used were of analytical reagent grade. The experimental studies were carried out at an ambient temperature of 30°C using freshly prepared solutions.

2.2. Synthesis of Activated Carbon Derived from Bagasse Precursor. The sugarcane bagasse used as the precursor for the adsorbent belongs to the *Saccharum sinense* species, which was obtained from an open market in Ota, Ogun State, Nigeria. The thick stalks were sliced in length of 150 mm and diameter of 15–30 mm. The stalks were cut into smaller sizes, and the hard-back was peeled off completely. The stalks were crushed, and the resulting juice extracted and washed with deionized water. The wet chaff was sun-dried for 9 h. The dried crushed stalk (bagasse) samples were milled into smaller sizes and sieved using a sieve shaker (SS-8R; Gilson Tapping, United States) whose mesh sizes ranged

from 0.1 mm to 1 mm. Particles within the range 0.1 mm–1 mm were collected and further treated by washing in deionized water three times. After that, the samples were dried in an oven (LDO-201-E; Vision Scientific, Japan) for 3 h at 95°C. After drying, the dried samples were immediately stored in airtight plastics for storage.

The chemically treated activated carbon (BAC) was synthesized using the protocols from the previous studies [29, 31] with some modifications. After preparation, the sugarcane bagasse powder was mixed with a 1.5 M H_3PO_4 and $ZnCl_2$, respectively, at an impregnation ratio of 1 : 1 by volume/weight, and then the impregnated mixtures were put in 500 mL beakers, covered, and stirred. The mixtures were left for 12 h for penetration of the activating agent into the precursor for proper surface modification. After the stipulated impregnation time, the resulting activated precursor slurry was filtered using the mousseline cloth. The residue obtained (activated bagasse) was then dried in the oven for a period of 3 h at a temperature of 115°C. The activated bagasse residues were withdrawn from the oven and immediately stored in plastic bags for the carbonization process.

The carbonization process for each of the treated precursors involved heating (in batches of 100 g) the samples in each crucible placed into a muffle furnace (Carbolite HTF 1700; Carbolite Gero, UK) at a temperature of 600°C for a period of 1 h. On withdrawal, the samples were allowed to cool to the room temperature of 30°C. The resulting activated carbon samples were rinsed with deionized water until the pH of the slurry tended toward 7, after which the carbon was dried in an oven for 3 h at 115°C and stored in airtight plastic containers for later use for the adsorption process.

2.3. Characterization of Derived Activated Carbons. Various properties of the activated carbon were obtained by standard procedures [32]. The moisture content of the BACs was determined by heating a known weighted sample in the oven (LDO-201-E; Vision Scientific, Japan) at 110°C for a period of 1 hr. The residues obtained were then ignited in the muffle furnace (Carbolite HTF 1700; Carbolite Gero, UK) at 750°C for a period of 8 h at a temperature of 900°C for 10 min to determine the ash content and volatile matter, respectively. Equation (1) shows the relationship between the ash content and the mass of each sample taken [33, 34]:

$$\text{ash } (\%) \frac{m_1}{m \times (100 - x)/100} \times 100, \quad (1)$$

where m_1 is the mass of ash, m is the mass of the tested sample, and x is the percentage of moisture content contained in the tested sample.

The Sear method was used to estimate the specific surface area (S) of the derived activated carbons with a few modifications [35]. 1.5 g of each activated carbon was agitated in 100 mL of dilute hydrochloric acid solution, set at a pH of 4. After that, 30 g of NaOH pellets were added to the suspension while agitation was taking place, and then the volume of the suspension was made up to 150 ml by adding deionized water. 0.1 N NaOH was titrated against the suspension while agitating to raise the pH from 4 to 9 after which the volume, V_{OH}, of NaOH was noted. The specific surface area, S, of the various adsorbents was estimated and is calculated as follows:

$$S = 32V_{OH} - 25. \quad (2)$$

The nitrogen adsorption and desorption experiments (Quantachrome NovaWin NOVA 2200E BET surface area analyzer) were further carried out to confirm and validate the specific surface area obtained from equation (2) using the Brunauer–Emmett–Teller (BET) surface area technique on the produced adsorbent samples.

The proximate analysis of both the adsorbents was done in line with standard procedures and practices as listed in ASTM [36].

The ability to be able to identify the surface characteristics/properties such as adsorbent crystallinity, pore and particle sizes, composition, and morphology is highly salient in understanding the role of the adsorbent in the adsorption process of Cu^{2+} from wastewater. The powder X-ray diffraction (XRD) patterns of the adsorbent samples were recorded with a Siemens D-500 X-ray diffractometer using a non-monochromated Cu Ka radiation source with a wavelength of 1.54 nm (30 kV, 15 mA) and a diffracted beam monochromator at room temperature. Scanning for crystallinity was performed between 2θ degrees of 2 and 70°. Scanning electron microscopy (SEM) analysis was carried out using an FEI Nova NanoSEM 400 scanning electron microscope operating at an accelerating voltage of 20 kV, equipped with an Oxford Inca energy dispersive X-ray spectroscopy (EDS) analysis detector unit in order to study the adsorbent morphology and composition, respectively. Zeta potential analysis of the produced adsorbents was carried out using an electrokinetic analyzer (SurPASS; Anton Paar) with a gap cell that is adjustable. The surface zeta potential was ultimately obtained in function of pH in a 0.001 M KCl electrolyte solution varying the solution pH by addition of 0.05 M HCl or 0.05 M NaOH through the automatic titration unit of the instrument. Different couples of samples were used for the acidic and basic titrations in order to avoid artifacts due to surface reactions during the measuring process. Three (3) measurements were carried out for each observed pH point. The surface functional groups of the BAC adsorbents were estimated using a Fourier transform infrared (FTIR) spectrometer (FTIR-8300; Shimadzu, Japan).

2.4. Batch Experiments. Stock solutions of copper(II) ions: (0.2, 0.4, 0.6, 0.85, and 1 g L^{-1}) were prepared by serial dilution from the concentrated stock solution. The influence of the experimental parameters such as contact time, pH, adsorbent dosage, and adsorbate dosage on the adsorption of Cu(II) ions from aqueous synthetic wastewater solutions was optimized in the batch experimental studies. The experimental setup includes 250 mL beakers, magnetic stirrers (UC152; Stuart Jergard, UK), a pH meter (HI 2210; Hanna, United States), a pipette, a glass funnel, sample bottles, and 150 μm Whatman filter papers. The setup consisted of a 200 mL mixture of the adsorbate and an optimized mass of both BACs in a beaker, of which the mixture is whirled with

the aid of a hot plate magnetic stirrer at a speed of 1000 rpm. The choice of whirling speed was to ensure homogenous pH distribution as well as a homogenous distribution of the adsorbent particles in the adsorbate solution. All these conditions were carried out at an ambient temperature of 30°C. The pH of the solutions was from 2 to 8 by adding 0.1 M HCl or 0.1 M NaOH to the samples as the experiment required. Subsequently, the process samples were collected solely by filtering the solution through a 150 μm Whatman filter paper, the absorbance of the filtrate was measured using a UV spectrophotometer (6405 UV-Vis; Jenway, UK) at a maximum wavelength (λ_{max}) of 600 nm and confirmed by using an atomic absorption spectrophotometer (VARIAN SpectrAA) at 20–400 nm. By using a five-data point standard calibration curve, the concentration of the copper(II) ions (based on the proportionality principle, as indicated in the Beer–Lambert's Law [37]) was measured. Various sets of experiments were successfully carried out in triplicate under the observed optimum conditions obtained. The overall sorption of the metal ion, q_e ($mg\,g^{-1}$), and percentage removal, R(%), onto the BACs were calculated using the mass balance:

$$q_e = \frac{(c_0 - c_e)V}{m_s}, \tag{3}$$

$$R\,(\%) = \frac{c_0 - c_e}{c_0} \times 100. \tag{4}$$

The batch kinetic studies were carried out similar to the method described in the batch equilibrium adsorption procedure. The aqueous samples were collected at regular intervals, and the concentrations of Cu(II) ions in the aqueous solutions were similarly measured. The sorption capacity, q_t ($mg\,g^{-1}$), at different contact times, t (min), is calculated using the following equation:

$$q_t = \frac{(c_0 - c_t)V}{m_s}, \tag{5}$$

where c_0, c_e, and c_t are the initial adsorbate concentration, adsorbate equilibrium concentration, and adsorbate concentration at time t (min), all measured in ($mg\,L^{-1}$); V represents the volume of solution (L); and m_s represents the dry mass of the BACs (g).

3. Results and Discussion

3.1. Surface Characterization of the Adsorbents. The physicochemical and proximate analyses of the prepared adsorbents in this study are illustrated in Table 1. The relationship between the surface area of a prepared activated carbon and its porosity has been characterized by a direct relationship. As shown in Table 1, the order of increase of surface areas of the derived activated carbons starting from the bagasse precursor was Bagasse < BAC-Zn < BAC-P. BAC-P could, therefore, be considered to give the best performance and also the most porous of all the adsorbents. Furthermore, the adsorbents possessed surface areas within the range of 10^0–10^3 m^2g^{-1}, hence confirming their conformity with the range expected of plant-based carbon adsorbents [38]. The Brunauer–Emmett–Teller (BET) surface area (S_{BET}), pore volume (V_T), and average pore diameter (D_p) of the BAC-P and BAC-Zn adsorbents before and after the adsorption process are illustrated in Table 2. It was observed that the BAC-P showed S_{BET} before and after adsorption of 427.5 m^2/g and 889.9 m^2/g, respectively, while BAC-Zn showed S_{BET} of 282 m^2/g and 588.8 m^2/g, respectively. The increase in specific surface area (S_{BET}) after the adsorption process could be attributed the complexation process during the adsorption process [39, 40]. Additionally, the activated carbons (BAC-P and BAC-Zn) prepared illustrate hysteresis loops, thereby indicating mesoporosity (Figure 1(a) and 1(b)); similar hysteresis loops were obtained by other researchers [39, 41–43]. As indicated in Table 2, the total pore volume (V_T) and micropore volume (V_{micro}) of the BAC-P and BAC-Zn adsorbents increased during and after the adsorption process most likely due to the formulation molecular complexes along the active sites of these adsorbents [41], thus showing a development of porosity. According to the IUPAC definition, the BAC-P and BAC-Zn pores were classified into three principal groups: micropores ($D_p < 2$ nm), mesopores ($2 \le D_p \le 50$ nm), and macropores ($D_p > 50$ nm). Table 2 and Figure 1(b) show the pore size distributions of the prepared adsorbent samples, indicating that the activated carbons principally include mesopores. The average pore diameters (D_p) for the activated carbons (before and after) were obtained to be between 2.11 and 2.14 nm; these results are in consonance with several previous studies [41, 43, 44]. It can also be asserted that the lower pH_{IEP} value of BAC-P than the pH_{IEP} value of BAC-Zn (3.63 and 5.26, respectively) in addition to the higher S_{BET} of BAC-P than that of BAC-Zn contributed greatly to

Table 1: Proximate analysis and physicochemical properties of the prepared adsorbents.

Physicochemical properties	Adsorbents		
	Bagasse	BAC-P	BAC-Zn
Surface area ($m^2\,g^{-1}$)	10	537	484
Bulk density ($g\,mL^{-1}$)	0.78	0.48	0.60
Iodine no. ($mg\,g^{-1}$)	132	201	175
pH	9.5	7.89	8.33
Proximate analysis			
Moisture content (%)	23.60	5.25	5.10
Ash content (%)	4.25	2.15	2.75
Volatile matter (%)	11.54	7.75	7.54
Fixed carbon (%)	61.45	10.72	12.75

Table 2: BET surface area, pore volume, and average pore diameter of BAC-P and BAC-Zn adsorbents.

	BAC-P		BAC-Zn	
	Before	After	Before	After
S_{BET} (m^2/g)	427.5	889.9	282.0	588.8
V_{micro} (cm^3/g)	0.175	0.318	0.118	0.225
V_{total} (cm^3/g)	0.258	0.454	0.173	0.330
D_p (nm)	2.14	2.11	2.13	2.13

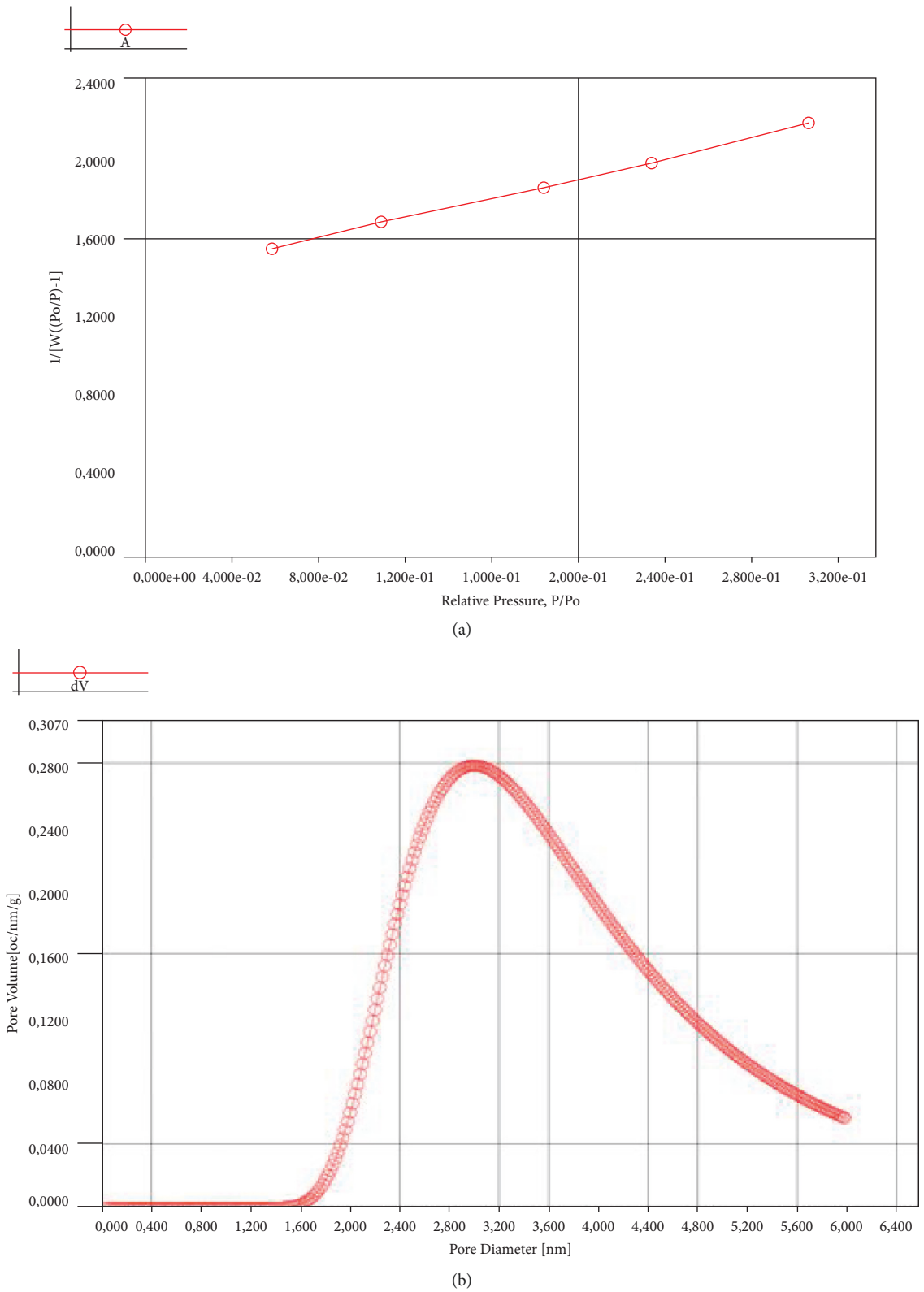

Figure 1: (a) BET surface area plot. (b) BJH desorption pore volume versus pore diameter of BAC-P adsorbent after adsorption.

the greater and more effective adsorption capacity of the BAC-P activated carbon over BAC-Zn [45].

It was also observed that BAC-P possessed the lowest bulk density, which accounts for its distinctive quality relative to BAC-Zn and bagasse. Therefore, BAC-P would provide a better contacting process for the adsorbate, thereby leading to a better effective adsorption system. The pH is a physicochemical property that affects the adsorption

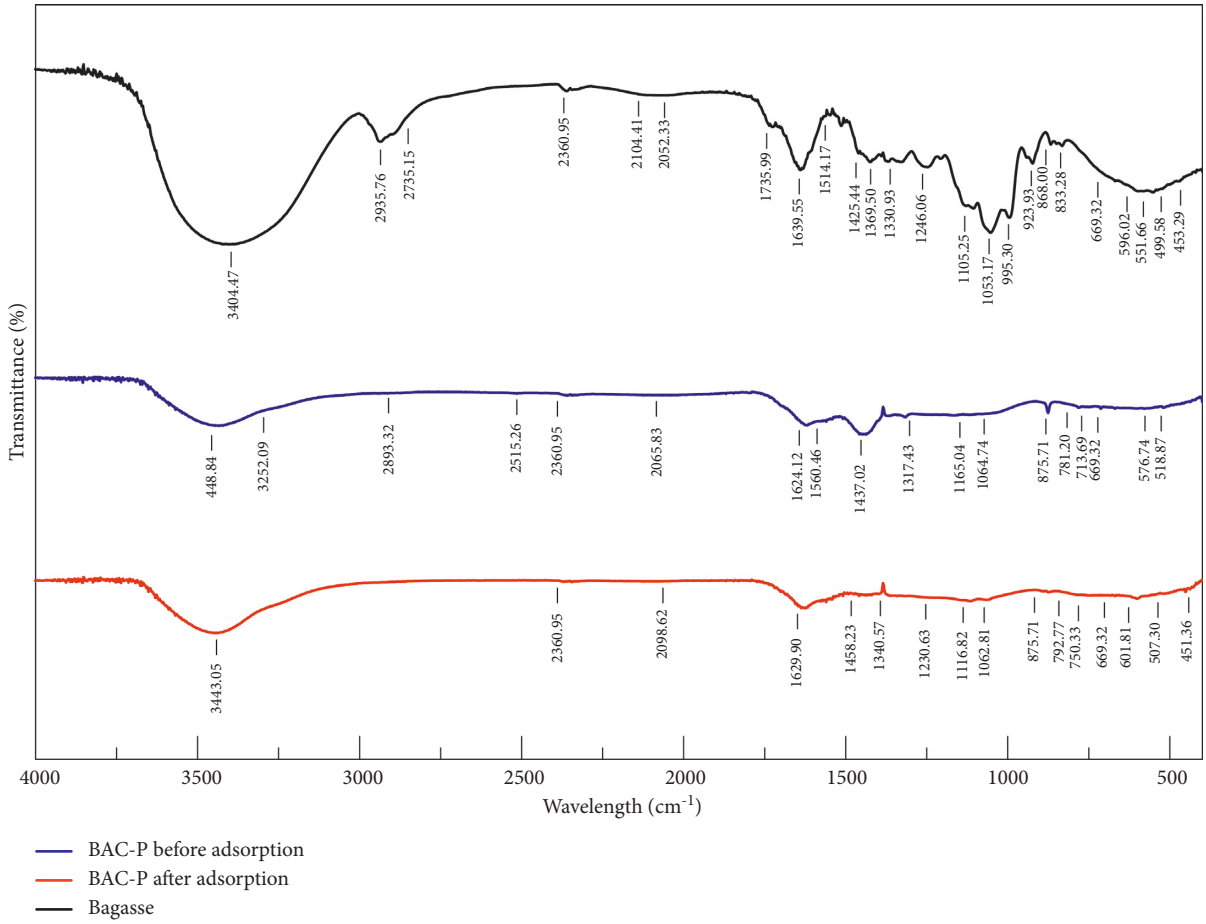

Figure 2: FTIR spectra of bagasse, BAC-P adsorbent before adsorption, and, BAC-P adsorbent after adsorption.

Table 3: FTIR main transitions showing different bonds present in sugarcane bagasse.

Wave number (cm^{-1})	Functional groups	Source
3404.47	O-H linked stretching of the hydroxyl group	Polysaccharides
2935.76	C-H symmetrical stretching	Polysaccharides
1735.99	C=O unconjugated stretching	Xylans
1639.55	C=C symmetrical stretching	Alkenes
1425.44	OH (water)	Water
1330.93	C-O aromatic ring	Cellulose
1105.25	C-O-C asymmetrical stretching	Cellulose
669.32	C-OH out-of-plane bending	Cellulose

capacity of heavy metals. The metal chemistry of various adsorbates as well as the subsequent functional groups located on each active site of the derived adsorbents being protonated could be affected by pH [46]. The pH values of the bagasse, BAC-Zn, and BAC-P were determined to be 9.5, 8.33, and 7.89, respectively. The results, as shown in Table 1, agreed with Cheremisinoff and Ellerbusch [38], whose work revealed that the pH of either raw or carbonized agricultural materials suspended in water was between the range of 4 and 12. The iodine value of an adsorbent is a basic property used in characterizing the effectiveness and ultimate efficacy of activated carbons. Jeyakumar and Chandrasekaran [33] illustrated the fact that iodine number can be used to determine the contents in the micropores of a prepared or derived adsorbent, which is obtained by the adsorption of the iodine molecules onto the surface of the adsorbent. The iodine numbers of bagasse, BAC-Zn, and BAC-P are given Table 1 with a higher iodine value indicating a higher degree of activation. The BAC-P had the highest iodine number of 201 mg g^{-1}, illustrating better development of its pore surface structure among the various adsorbents.

The proximate analysis of the adsorbents is also illustrated in Table 1. The moisture content of BAC-P and BAC-Zn was 5.25 and 5.10%, respectively. The moisture content of these adsorbents signifies that they could be adjudged to give an adsorption performance with great quality since it has been established that a lower moisture content greatly increases the capacity of carbon adsorbents to adsorb on their

Table 4: FTIR spectral analysis of BAC-P and BAC-Zn adsorbents.

Peak	Frequency (cm^{-1})		Difference	Assignment
	Before adsorption	After adsorption		
		BAC-P adsorbent		
1	3448.84	3443.05	−5.79	O-H stretch of hydroxyl group
2	2065.83	2098.62	+32.79	C-O group in alcohol
3	1624.12	1629.90	+5.78	C=O stretch of carboxylic acid
4	1437.02	1458.23	+21.21	C=C bond of aromatic ring
5	1165.04	1116.82	−48.22	C≡C bond of alkyne group
6	1064.74	1062.81	−1.93	C=O=C stretch of polysaccharides
7	781.20	792.77	+11.57	C-H stretch of aliphatic alkanes
		BAC-Zn adsorbent		
1	3441.12	3448.84	+7.72	O-H stretch of hydroxyl group
2	2050.40	2060.04	+9.64	C-O ring in alcohol
3	1616.40	1624.12	+7.72	C=O stretch of carboxylic acid
4	1435.09	1438.94	+3.85	C=C bond of aromatic ring
5	1186.26	1116.82	−69.44	C≡C bond of alkyne group
6	—	1070.53	—	C=O=C stretch of polysaccharides
7	781.20	754.19	−27.01	C-H stretch of aliphatic alkanes

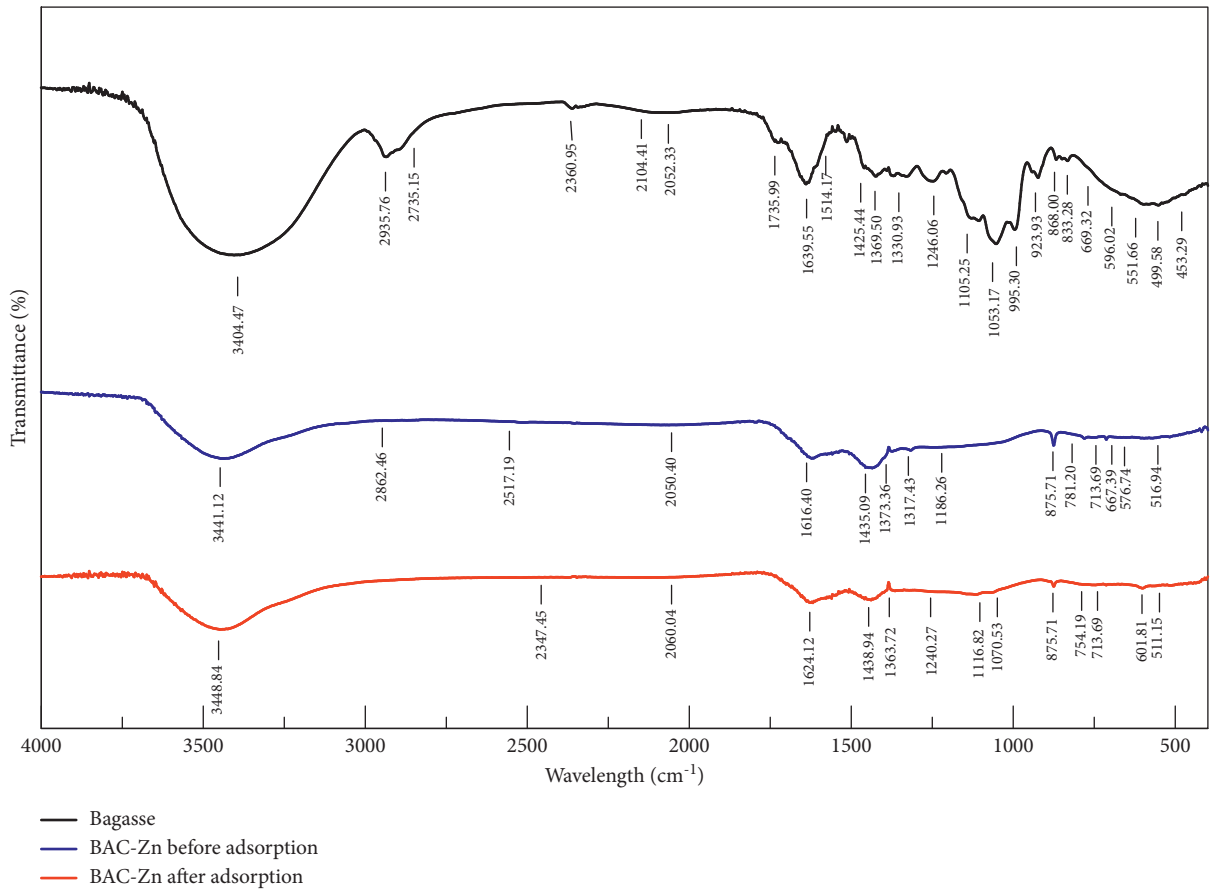

Figure 3: FTIR spectra of bagasse, BAC-Zn adsorbent before adsorption, and BAC-Zn adsorbent after adsorption.

active sites, thereby concentrating the action of the adsorbents. The ash content of BAC-P was 2.15%, which was the least among adsorbents that were duly investigated, as the ash content decreases, the better the starting material for the removal of heavy metal ions from industrial wastewater [47]. Therefore, BAC-P was found to be a better adsorbent than the bagasse and BAC-Zn. As stated by Khan et al. [48], the least ash content value of BAC-P was favourable because the ash content can interfere with the efficacy of the adsorption process. The volatile matter of BAC-P and BAC-Zn was very low compared with the sugarcane bagasse. This can easily be attributed to the fact that as thermal activation was

performed, the pyrolysis process led to the elimination of most of the noncarbon elements such as $N_{2(g)}$, S, $H_{2(g)}$, and $O_{2(g)}$ as volatile by-products [30]. The fixed carbon content of the sugarcane bagasse was obtained as 61.45%, while that of BAC-P and BAC-Zn was then obtained as 10.72 and 12.75% with a %error of $\pm 3.15 < \pm 5$, respectively. Therefore, these results show that both BAC-P and BAC-Zn adsorbents are feasible and possible options for activated carbon production.

3.1.1. Fourier Transform Infrared (FTIR) Characterization of Prepared Adsorbents. The FTIR spectra of the prepared adsorbents were observed within the range of 4000 to 400 cm^{-1}. The FTIR spectra of the sugarcane bagasse, BAC-P adsorbent before adsorption, and the BAC-P adsorbent after adsorption are shown in Figure 2, illustrating the surface functional groups being detected. Table 3 shows the following surface functional groups being identified for the sugarcane bagasse precursor [49, 50]. The 3404.47 cm^{-1} peak was related to vibrations ν (O-H) in hydroxyl functional groups of polysaccharides, signifying a lignocellulolytic composition of the bagasse. Weak bands at 2935.76 and 2735.15 cm^{-1} were attributed to polysaccharides and aliphatic bonds, respectively. In addition, the broadband spectrum peaks of 1130.93 cm^{-1}, 1105.25 cm^{-1}, and 923.93 cm^{-1} revealed the existence of vibrating C-O aromatic rings, asymmetric stretching of the C-O-C bonds, and an out-of-plane C-OH group, respectively, all corresponding to a cellulolytic source [50]. The FTIR spectra of the BAC-P adsorbent before and after adsorption are shown in Figure 2. The FTIR spectrum of the BAC-P adsorbent before Cu(II) ion adsorption indicates peaks at 3448.84 cm^{-1} due to O–H stretching in the hydroxyl functional group, the peak at 1624.12 cm^{-1} shows C=O stretching of carboxylic acid [51, 52], the band peak observed at 1437.02 cm^{-1} is C=C group attributed to the bonding of aromatic rings, while the band at 1165.04 cm^{-1} indicates the presence of C≡C triple bonds of alkynes [53, 54], and the 1064.74 cm^{-1} peak is ascribed to C=O=C polysaccharide stretching vibration [4, 26]. The peak at 781.20 cm^{-1} was ascribed as the C–H group stretching of aliphatic alkanes, and that at 2065.83 cm^{-1} was due to C-O group stretch of alcohol [55]. The differences in the intensity of the peaks of the spectral analysis for the various functional groups that could be the possible sites for the Cu(II) ions adsorption are shown in Table 4. The FTIR spectrum of the BAC-Zn adsorbent is presented in Figure 3. The peak at 3441.12 cm^{-1} is attributed to O-H group stretching in the activated carbon polymer bond, while the peaks at 1186.26 cm^{-1} and 1070.53 cm^{-1} are assigned to C≡C stretch bond of the alkyne group and C=O=C stretch of polysaccharides, respectively. Furthermore, the peak at 2050.40 cm^{-1} indicates the C-O ring stretch of alcohol, and the band peak at 781.20 cm^{-1} is because of C-H stretching of aliphatic hydrocarbons (alkanes) [54]. The band at 1616.40 cm^{-1} shows C=O stretching of the carboxylic acid group [56], and that of 1435.09 cm^{-1} is because of C=C of aromatic ring bonds [57]. Also, the band peak obtained at 1317.43 cm^{-1} is because of the stretching vibration of C=O in the carboxyl group [58]. Correspondingly, the changes in the peak intensities of the spectral analysis for the various functional groups of the BAC-Zn adsorbent are also indicated in Table 4, which consequently could also be the possible sites for Cu(II) ion adsorption.

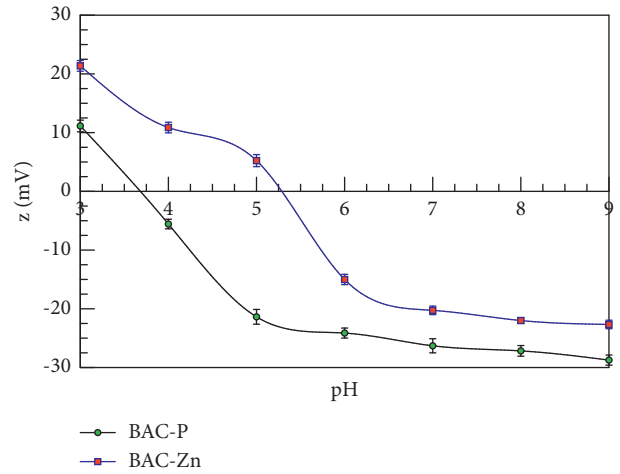

Figure 4: Zeta potential of BAC-P and BAC-Zn adsorbents. Error bar shown is the standard deviation of the mean.

3.1.2. Zeta Potential Measurement. The zeta potential measurements are characterization techniques largely used for the characterization of colloidal suspensions and nanoparticles in order to ascertain the potential difference between the adsorptive and desorptive layers bound on the particle surface in a solid-liquid adsorption system [40, 59]. The isoelectric point (pH_{IEP}) of solid or protein is the pH of a solution in which the net charge/zeta potential of the said solution becomes zero [60]. The surface of the particle will be essentially/largely negatively charged at solution $pH > pH_{IEP}$, giving rise to like-charged molecules exhibiting repulsion, while at solution $pH < pH_{IEP}$, the surface of the solid is mostly positively charged also displaying repulsive forces among the molecules [40, 61]. The zeta potential of BAC-P decreased from 11.14 to 28.73 mV, while that of BAC-Zn declined from 21.37 to 22.67 mV as the pH of the solution increased from 3 to 9 as shown in Figure 4. The pH_{IEP} values of BAC-P and BAC-Zn were 3.63 and 5.26, respectively (Figure 4). Furthermore, the zeta potential and subsequent pH_{IEP} values of BAC-P were verifiably smaller than those of BAC-Zn, at the same solution pH; this phenomenon being corroborated by Tang et al. [40] established the most likely reason why the BAC-P adsorbent had a better adsorption capacity compared with BAC-Zn. In addition, as the initial pH of the solution was lower or higher than the $pH_{IEP,}$ the adsorption of Cu^{2+} onto the surface of the produced adsorbents can be attributed to ion exchange or electrostatic attraction with molecular complexation.

3.1.3. X-Ray Diffraction Analysis. X-ray diffraction analysis is a very important analytical technique commonly used in determining and verifying the crystalline phase of powdered

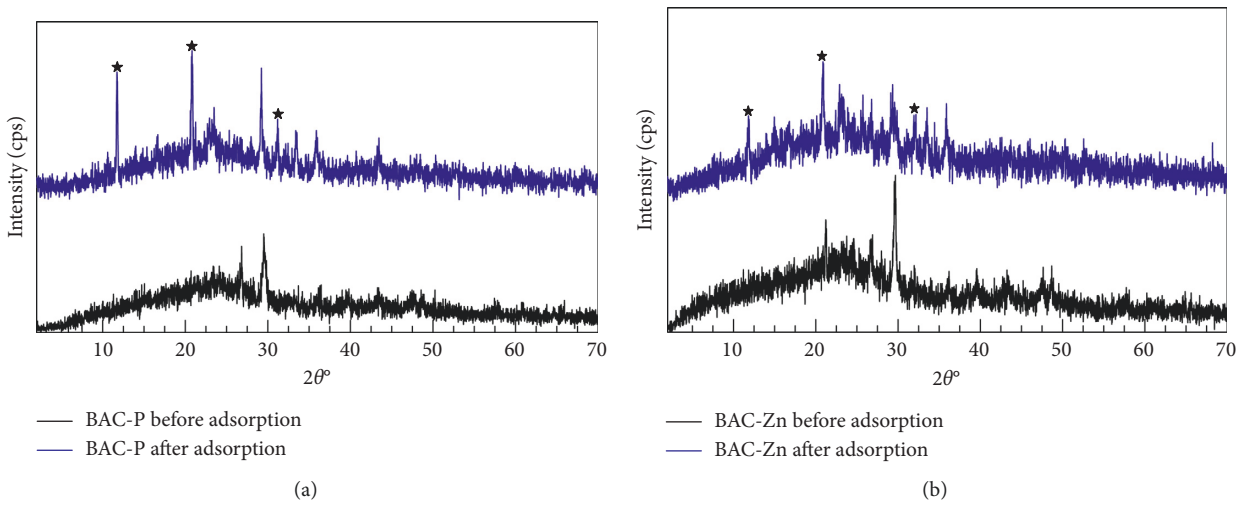

Figure 5: The XRD Patterns showing the (a) BAC-P adsorbent and (b) BAC-Zn adsorbent, before and after adsorption.

materials and to identify the framework lattice of such particular materials [62, 63]. The compared powder X-ray diffraction analysis of the BAC-P and BAC-Zn adsorbents (before and after adsorption) is shown in Figures 5(a) and 5(b), respectively. The powder X-ray diffractograms of BAC-P and BAC-Zn adsorbents after the adsorption process are indistinguishable and identical to that of the host adsorbents (BAC-P and BAC-Zn before adsorption) framework lattice [31]. The host adsorbents (BAC-P and BAC-Zn before adsorption) were observed to have two major diffraction peaks between $2\theta^{\circ} = 2–70^{\circ}$ at 26.2° and 29.5° for the BAC-P adsorbent and 26.1° and 29.7° for BAC-Zn adsorbent, matching the observations of El-Azazy et al. [63] and Thuan et al. [31]. After the adsorption of Cu^{2+}, the XRD patterns of BAC-P and BAC-Zn after adsorption showed a major difference in the compared diffractograms (Figures 5(a) and 5(b)); these differences were observed to be additional Bragg peaks at 12°, 21.5°, and 31.5° for BAC-P, while for the BAC-Zn adsorbent, the additional peaks observed were at 12°, 21.5°, and 31.7° as indicated by " ∗ ", which is readily assignable to the presence of Cu^{2+} ions on the surface of the BAC-P and BAC-Zn adsorbents [4, 64, 65]. Furthermore, the XRD diffractograms, which were taken before and after adsorption in Figures 5(a) and 5(b), indicate that there are no appreciable changes in the spectra (except for the additional peaks illustrating the adsorption of Cu^{2+}) and no Bragg peaks indicating impurity were detected [39]. As validated by Dash et al. [39] and El-Azazy et al. [63], this phenomenon reveals that the Cu^{2+} ions adsorbed onto the prepared activated carbons did not change the chemical structure of the adsorbents and maintained the crystallinity of the BAC-P and BAC-Zn adsorbents and the adsorption process is physical in nature [66].

3.1.4. Morphological Characteristics: SEM and EDX Analyses. The surface morphology, microporosity, and elemental features and compositions of both adsorbents were visualized using the SEM and SEM-EDX analyses. Figures 6(a)-6(d) display the SEM micrographs for BAC-Zn and BAC-P adsorbents before and after adsorption. The backscattered electron diffraction SEM in Z-contrast mode (BSED-SEM) micrographs show the evidence of the presence of different types of irregular pores (micro- and mesopores) across the surface of the prepared activated carbons, which was also confirmed by the BET analysis as stated above (Section 3.1). Figures 6(b) and 6(d) show that the Cu^{2+} nanoparticles appear to have been adsorbed on the surface as a white shining area across the BAC-Zn and BAC-P adsorbents after adsorption, with other analytical characterization techniques employed to confirm this phenomenon. The SEM observations and findings were further confirmed using the EDX analysis as shown in Figures 7–10. The EDX analysis of the BAC-P revealed that the white shining area across its surface was indeed Cu(II) being deposited/adsorbed on the surface of the adsorbent. The EDX analysis of BAC-P showed a high atomic concentration of carbon (83.56%) and oxygen (16.44%), authenticating the formation of carbonaceous material following the chemical treatment of biomass [63]. The adsorption of Cu^{2+} on the surface of BAC-P adsorbent was also confirmed by the EDX analysis of the activated carbon as shown in Figure 8(b), revealing that about 6.56% of Cu(II) ions was adsorbed onto the BAC-P surface, while Figure 10(b) shows that 16.77% of Cu(II) ions was adsorbed onto the BAC-Zn surface. These results and findings are in good agreement with analogous studies that were previously reported [8, 31, 67].

3.2. Dynamics of Cu(II) Ions Adsorption onto Prepared Adsorbents

3.2.1. Effect of Contact Time on the Removal of Cu(II) Ions. A major operational parameter for the efficient and economical treatment of industrial wastewater is equilibrium time; due to the dynamicity of the adsorption process, the

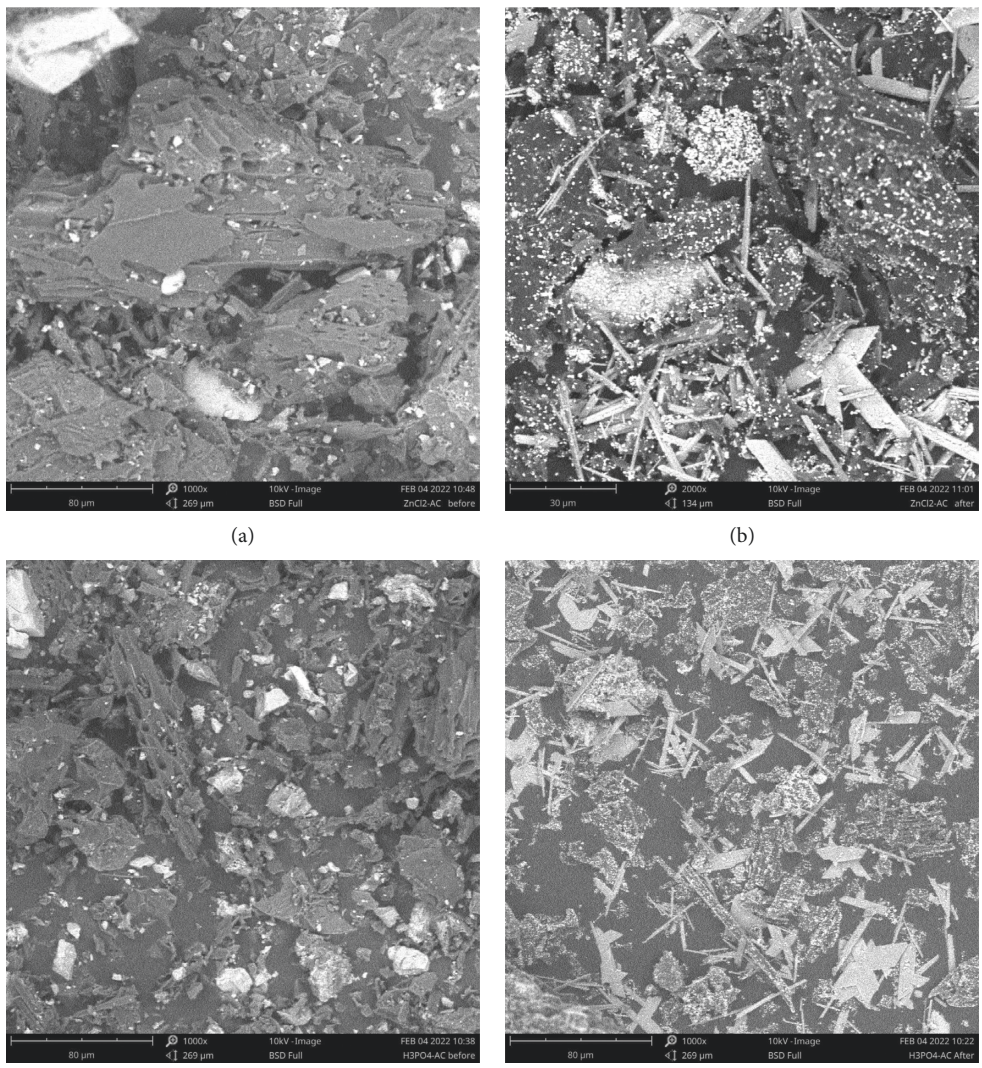

(a) (b) (c) (d)

Figure 6: SEM micrographs of the BAC-P and BAC-Zn adsorbent particles showing (a) BSED image at 1000× of BAC-Zn before adsorption, (b) BSED image at 2000× of BAC-Zn after adsorption, (c) BSED image at 1000× of BAC-P before adsorption, and (d) BSED image at 1000× of BAC-P after adsorption.

contact time was studied based on the idea of Sabela et al. [44] with some modifications. In Figure 11, it was observed that the rate of adsorption increased drastically at the start of the experiment up until the first hour based on the sharp slope associated with percentage (%) removal of the Cu(II) adsorbate ions. This is most likely due to an initial high sorption potential between the adsorbate in solution and adsorbent caused by the high concentration gradient [44, 68]. From Figure 11, the rate of removal began to gradually drop till a plateau was reached where no further removal was observed, i.e., the increase in agitation time led to more coverage of the adsorbent pore spaces with Cu(II) ions until the equilibrium of the adsorption process was established. This is because of the progressive decrease in the electrostatic force of attraction between the adsorbate ions and the active sites of the adsorbent as the surface of the activated carbons get saturated [69]; hence, the copper ions tend to diffuse to get to the surface of the adsorbent [70]. The decline in the %removal of Cu(II) ions in the BAC-P adsorbent sorption process is due to a desorption phenomenon that could have been caused by the whirling/agitation speed of the mixture, hence leading to the dispersal of the adsorbate molecules back into the solution. Some of the distinctive features between the BAC-Zn and BAC-P sorption activities are the equilibrium time when using BAC-P as an adsorbent came quicker (twice as fast) relative to using BAC-Zn adsorbent for the adsorption process.

3.2.2. Effect of Adsorbent Dosage on the Removal of Cu(II) Ions. The effect of adsorbent loading on the process of adsorption is very critical in determining the optimum dosage required for the removal of the highest possible amount of the contaminant (Cu(II) ions) in a given volume of a contaminated solution as illustrated in Figure 12. The optimum dosage is the adsorbent dose that is most

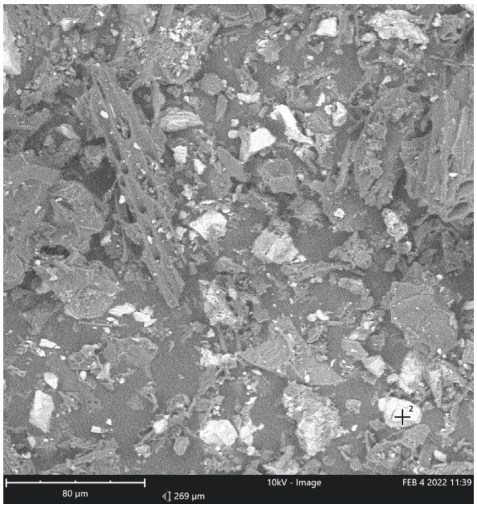

(a)

Element Number	Element Symbol	Element Name	Atomic Conc.	Weight Conc.
6	C	Carbon	83.56	79.23
8	O	Oxygen	16.44	20.77
		Total	100	100

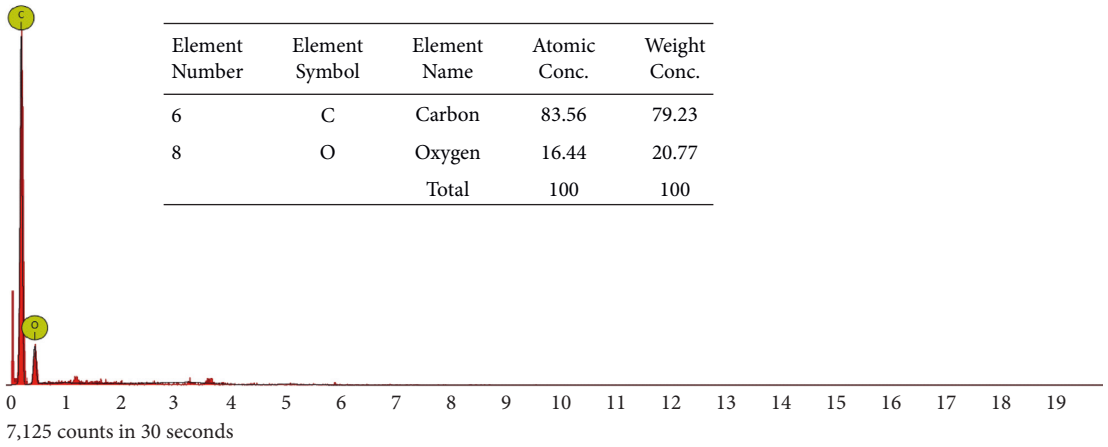

(b)

Figure 7: (a) BSED image of the BAC-P adsorbent before adsorption showing the spectrum used for EDX analysis. (b) The corresponding EDX spectrum at the spectrum point as indicated in (a).

economically viable such that below this dosage, the most effective removal is not achieved, and above this optimum dosage, there would be wastage of adsorbent. In Figure 12, strict observation showed that the percentage removal of the adsorbate rose sharply at the start, as the dose of the adsorbent was varied between 0 and 20 g L^{-1}, keeping all other operational parameters (pH, agitation speed, contact time, initial ion concentration, and particle size) constant. This observation concurred with that of the previous studies [44, 70, 71]. The highest Cu(II) removal percentage/efficiency for BAC-Zn and BAC-P was 56.8% and 82.4%, respectively, at an adsorbent dosage of 20 g, thus indicating that the surface area of the activated carbons also has a principal main effect on the efficacy of the removal of Cu(II) ions from synthetic industrial water. Therefore, the increasing order of the specific surface area of the derived adsorbents and therefore Cu(II) ions percentage removal is bagasse < BAC-Zn < BAC-P [51, 63]. These observations can be associated with the sharp increase in the number of adsorption sites available, therefore facilitating more effective adsorbate removal from the solution. As a plateau was approached, the increase in dosage was halted due to the ineffectiveness in adsorbate removal, as a result of a conglomeration of the carbon granules, thereby limiting the diffusion path. Distinctive features observed between BAC-P and BAC-Zn experiments were that at dosages higher than 10 g L^{-1} for the BAC-Zn adsorbent, no further improvement of %removal was observed, while in the case of the BAC-P adsorbent, %removal was relatively negligible with optimal dosages of 9 g L^{-1} and 5 g L^{-1}.

3.2.3. Effect of pH on the Removal of Cu(II) Ions. The carbon molecule being amphoteric in nature, [72, 73] has its sorption activities on its surface greatly influenced by the pH of the industrial wastewater. As other operational parameters (adsorbent dosage, agitation speed, contact time, initial metal ion concentration) were kept constant, the effect of pH ($2.0 \leq pH \leq 8.0$) values on the adsorption of Cu(II) ions onto BAC-P and BAC-Zn is shown in Figure 13. The choice of the range used was adapted and relatively modified from the work of Albrecht et al. [74] because beyond the pH of 8 the

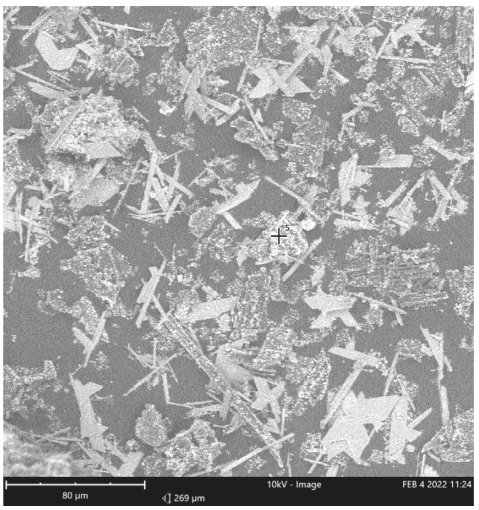

(a)

Element Number	Element Symbol	Element Name	Atomic Conc.	Weight Conc.
6	C	Carbon	88.37	62.51
29	Cu	Copper	6.56	24.54
16	S	Sulfur	4.32	8.16
47	Ag	Silver	0.75	4.79
		Total	100	100

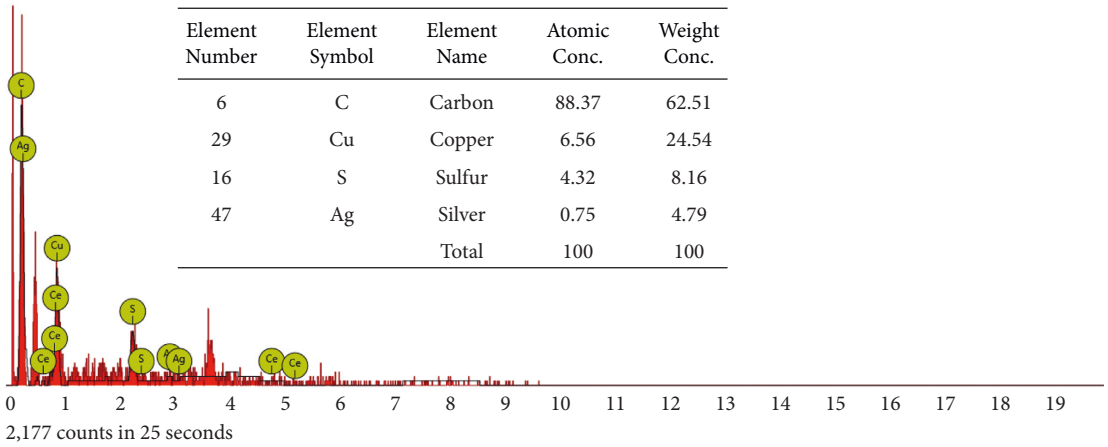

(b)

Figure 8: (a) BSED image of the BAC-P adsorbent after adsorption showing the spectrum used for EDX analysis. (b) The corresponding EDX spectrum at the spectrum point as indicated in (a).

precipitation of Cu(II) ions was observed [75]. From Figure 13, the curve trend indicated that the maximum adsorbate removal was attained at pH of 5 and 4 for BAC-Zn and BAC-P, respectively. It was observed that, as the pH increased steadily from the value of 2, there was a resultant increase in the %removal of copper(II) ions; this was because at low pH values, and there is competitive adsorption between the H^+ and the target adsorbate Cu^{2+} ions, hence the difficulty in the Cu^{2+} sorption onto the active sites [44, 76]. The least %removal was at pH 2 in both cases of the BAC-P and BAC-Zn experiments. From pH 2 to 3, a sharp increase in adsorbate removal was observed, and this could be because of the sudden reduction in the concentration of the H^+ ions present in the solution, hence making adsorption sites readily available for the target adsorbate. At pH value >5, a less sharp decline in adsorbate removal was observed most likely because the Cu(II) ion precipitate ($Cu(OH)_2$) becomes prevalent in the solution and therefore sediment, making the metal ions less available for the adsorption process [74, 77].

3.2.4. Kinetic Modeling of Cu(II) Ions Adsorption. The kinetic process depicts the time rate of change of concentration of the interacting materials, i.e., either the product or the reactants. In chemical reactions, it is a chemical process that involves the disintegration of molecules or atoms for the formation of new ones, thereby causing changes in the concentrations of the molecules or materials present. In physical processes like adsorption, it just involves the migration of molecules or atoms from a region of less stability to regions of higher stability under the influence of electrostatic and Van der Waals forces, which are physical forces. For the study of the kinetics of the different adsorbents used for the experiment, the fractional power model, pseudo-first-order [78] model, pseudo-second-order kinetic model, the intraparticle diffusion (IPD) (or Weber and Morris) model [79], Elovich kinetic model, and Boyd kinetic model were used to investigate the adsorption data obtained.

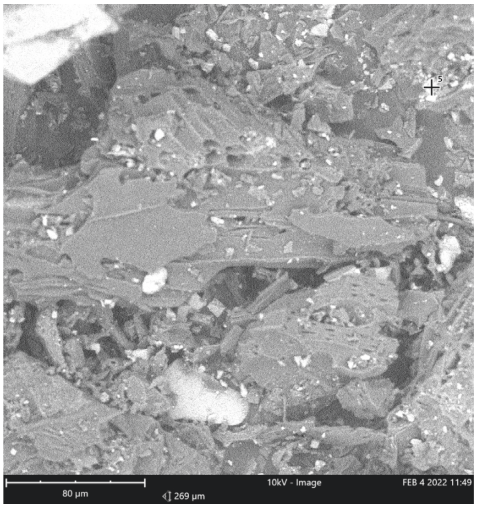

(a)

Element Number	Element Symbol	Element Name	Atomic Conc.	Weight Conc.
6	C	Carbon	62.01	44.54
20	Ca	Calcium	11.96	28.65
8	O	Oxygen	25.71	24.60
48	Cd	Cadmium	0.32	2.21
		Total	100	100

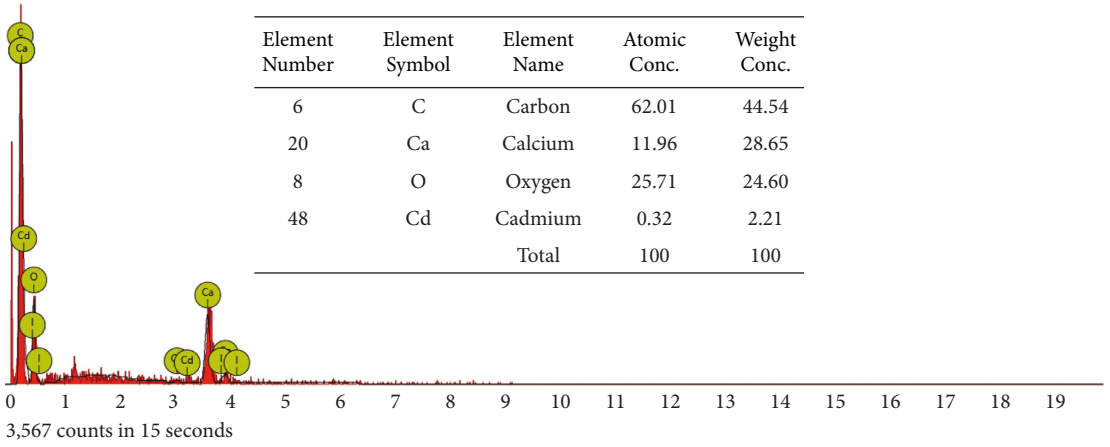

(b)

Figure 9: (a) BSED image of the BAC-Zn adsorbent before adsorption showing the spectrum used for EDX analysis. (b) The corresponding EDX spectrum at the spectrum point as indicated in (a).

The fractional power model, as shown in equation (6), indicates the uptake of metal ions increases exponentially with time:

$$q_t = k_f t^v. \tag{6}$$

Linearizing equation (6) by taking the natural logarithm gives equation (7):

$$In\, q_t = In k_f + v\, In t. \tag{7}$$

Hence, from equation (7), various parameters can be obtained by making the linear plot of $In\, q_t$ versus $In\, t$.Here, q_t is the amount of adsorbate ($mg\, g^{-1}$) adsorbed at a particular point in time t, k_f is the fractional power kinetic model constant (mg g^{-1}), v is fractional power model kinetic model exponent (min^{-1}), and t is time (h).

The linearized form of the pseudo-first-order model, as indicated in equation (9) obtained from equation (8), is given as follows:

$$\frac{dq_t}{dt} = k_1 (q_e - q_t), \tag{8}$$

$$In(q_e - q_t) = In q_e - k_1 t, \tag{9}$$

which leads to a straight line plot of $In\ (q_e - q_t)$ versus t, with a slope k_1 as the specific rate constant of the Lagergren pseudo-first-order kinetics sorption (L min^{-1}) and an intercept $In\ (q_e)$.

The pseudo-second-order kinetic model is given by

$$\frac{dq_t}{dt} = k_2 (q_e - q_t)^2. \tag{10}$$

The integrated form of equation (10) is obtained as follows:

$$q_t = \frac{k_2 q_e^2 t}{1 + k_2 q_e t}. \tag{11}$$

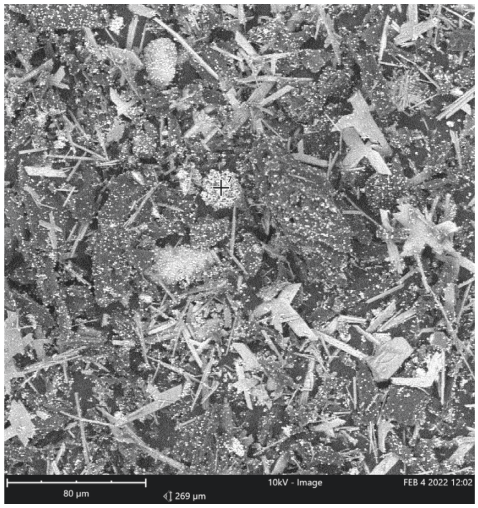

(a)

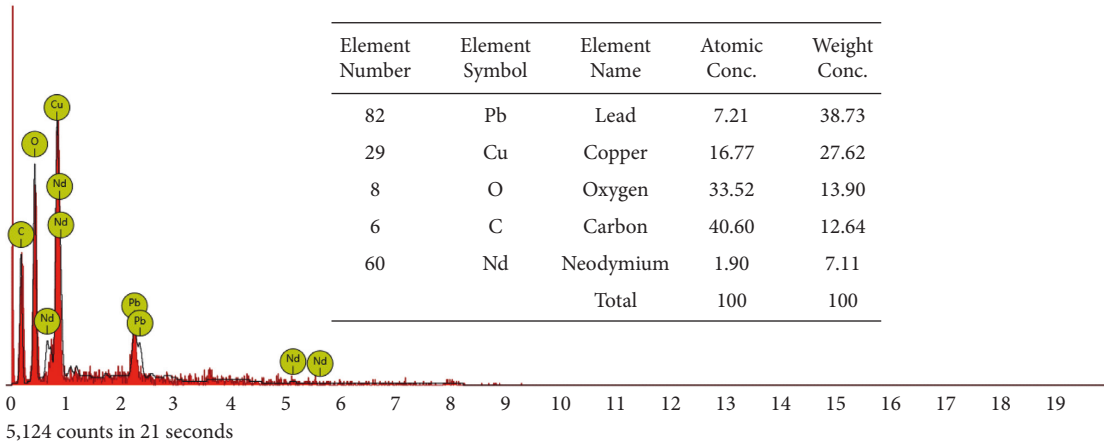

Element Number	Element Symbol	Element Name	Atomic Conc.	Weight Conc.
82	Pb	Lead	7.21	38.73
29	Cu	Copper	16.77	27.62
8	O	Oxygen	33.52	13.90
6	C	Carbon	40.60	12.64
60	Nd	Neodymium	1.90	7.11
		Total	100	100

(b)

Figure 10: (a) BSED image of the BAC-Zn adsorbent after adsorption showing the spectrum used for EDX analysis. (b) The corresponding EDX spectrum at the spectrum point as indicated in (a).

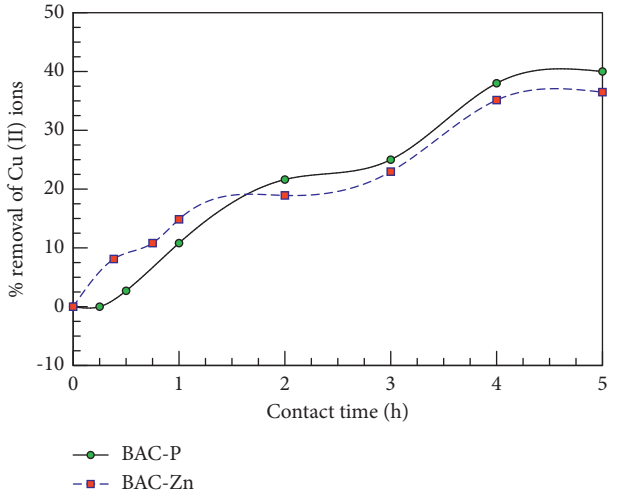

Figure 11: Effect of contact time on the removal efficiency of Cu(II) ions using BAC-P and BAC-Zn at $c_0 = 1$ g L^{-1}, pH = 4.5, dose of each adsorbent = 1 g, agitation speed = 150 rpm, contact time = 300 min, particle size = 250 μm, and temperature of solution = 30°C.

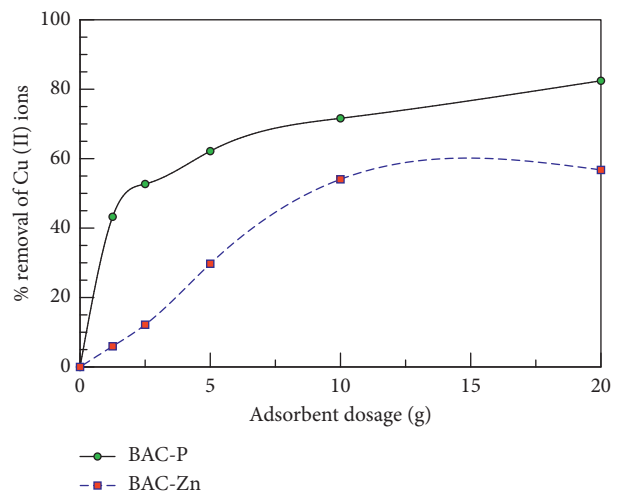

Figure 12: Effect of adsorbent dosage on the removal efficiency of Cu(II) ions using BAC-P and BAC-Zn at $c_0 = 1$ g L^{-1}, pH = 4.5, agitation speed = 150 rpm, contact time = 300 min, particle size = 250 μm, and temperature of solution = 30°C.

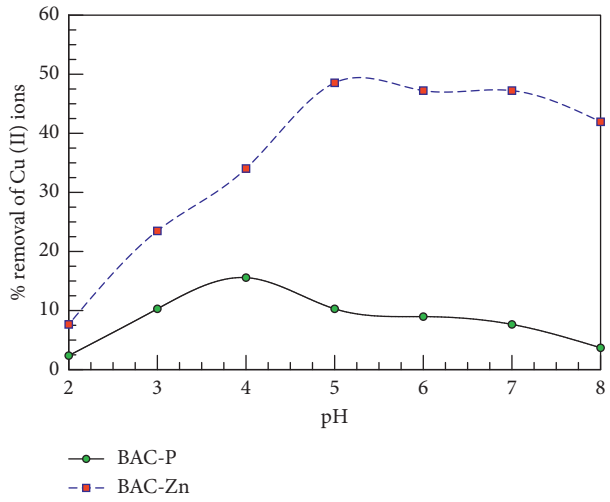

Figure 13: Effect of pH on the removal efficiency of Cu(II) ions using BAC-P and BAC-Zn at $c_0 = 1$ g L^{-1}, agitation speed = 150 rpm, dose of each adsorbent = 1 g, contact time = 300 min, particle size = 250 μm, and temperature of solution = 30°C.

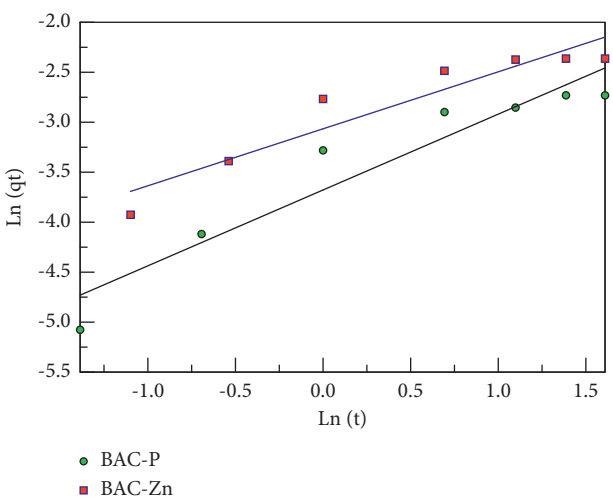

Figure 14: Fractional power model kinetics for adsorption of 1 g L^{-1} Cu(II) ions onto the BAC-P and BAC-Zn adsorbents.

Furthermore, equation (11) serves as a basis for various forms of linearized equations. One of which is used in this research work:

$$\frac{t}{q_t} = \frac{1}{k_2 q_e^2} + \frac{1}{q_e} t. \tag{12}$$

Therefore, a plot of t/q_t versus t should yield a straight line from which the slope and intercept q_e and k_2 are obtained, respectively.

The intraparticle diffusion (IPD) model [79] is used to understand the mechanism of diffusion involved in the adsorption process. The Weber and Morris model is expressed as follows:

$$q_t = k_{ip} t^{1/2} + c. \tag{13}$$

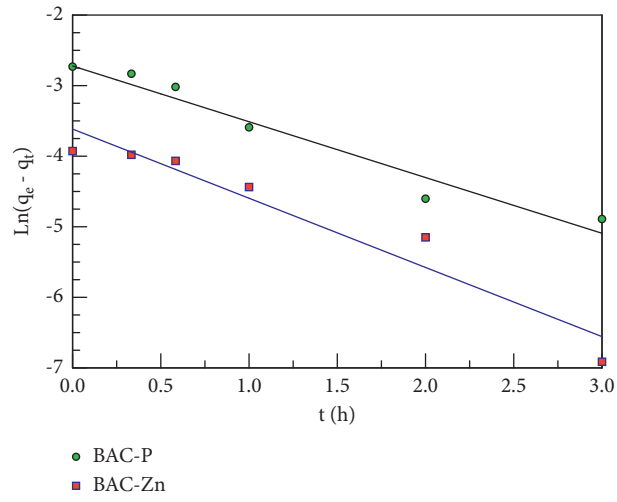

Figure 15: Pseudo-first-order kinetics for adsorption of 1 g L^{-1} Cu(II) ions onto the BAC-P and BAC-Zn adsorbents.

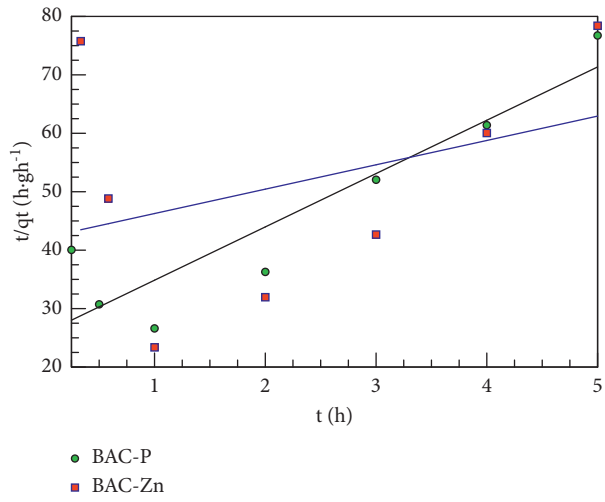

Figure 16: Pseudo-second-order kinetics for adsorption of 1 g L^{-1} Cu(II) ions onto the BAC-P and BAC-Zn adsorbents.

From equation (13), c would be obtained as intercept, and the intra-particle diffusion rate constant k_{ip} (mg g.min$^{-0.5}$) would be obtained as the slope from the linear plot of uptake (q_t) versus the square root of time ($t^{1/2}$).

The Elovich rate equation [73] is based on the adsorption capacity of an adsorbent being typically used to depict the chemisorption kinetics of gases on heterogeneous solids. However, due to its limiting property of not being able to capture the slow kinetics of adsorption processes, the Elovich model is quite restricted in usage [80]. The Elovich rate equation is expressed as follows:

$$\frac{dq_t}{dt} = \alpha_e \exp(-\beta_e q_t), \tag{14}$$

where α_e and β_e are the experimental constants. As $q_t \longrightarrow 0, dq_t/dt \longrightarrow \alpha$; hence, α_e is regarded as the initial rate of adsorption and β_e is the Elovich kinetic model

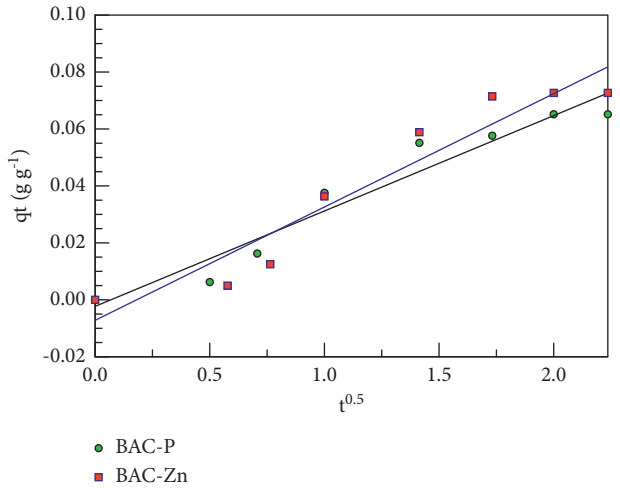

Figure 17: Intraparticle diffusion kinetics for adsorption of 1 g L^{-1} Cu(II) ions onto the BAC-P and BAC-Zn adsorbents.

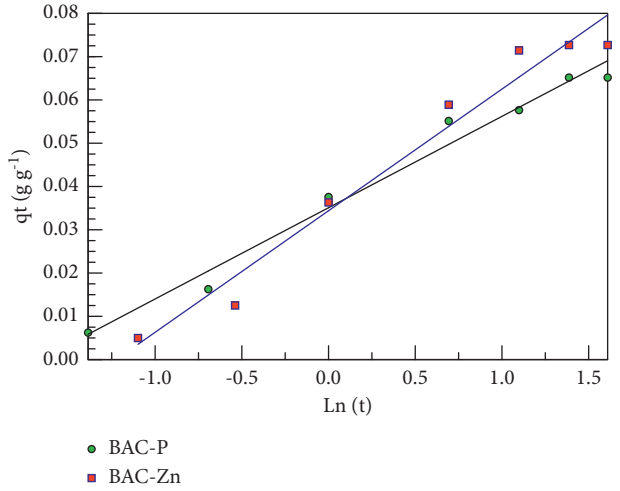

Figure 18: Elovich kinetics for adsorption of 1 g L^{-1} Cu(II) ions onto the BAC-P and BAC-Zn adsorbents.

constant (g mg^{-1}). When $t = 0, q_t = 0$, and $t = t, q_t = q_t$, and when equation (14) is integrated, we obtain

$$q_t = \frac{1}{\beta_e} In(\alpha_e \beta_e) + \frac{1}{\beta_e} Int. \quad (15)$$

Hence, a linear plot of q_t against $In\, t$ can be made, with a slope of $1/\beta_e$ and an intercept of $(1/\beta_e)In(\alpha_e\beta_e)$.

The goodness-of-fit results in Figures 14–19 were substantiated and justified as a result of the closeness of the coefficients of determination to unity. Table 5 presents the estimated kinetic parameters and their subsequent R^2 values.

The fractional kinetic model was fitted with the kinetic data, as shown in Figure 14. Here, the value of the exponent, v, was less than 1, indicating the time dependence of the adsorption of Cu^{2+} ions onto BAC-P and BAC-Zn adsorbents. As illustrated in Table 5, the fractional power kinetic model did not provide a relatively good fit to the kinetic data of the adsorption process, as the R^2 values in both the adsorbents were not close to unity.

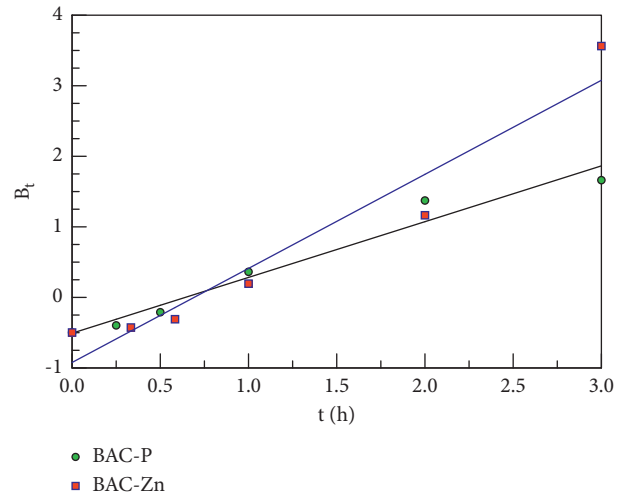

Figure 19: Boyd plot for adsorption of 1 g L^{-1} Cu(II) ions onto the BAC-P and BAC-Zn adsorbents.

Furthermore, the experimental kinetic plot did not show a satisfactory fit (Figure 16) to the pseudo-second-order kinetic model since the coefficient of determination (R^2) values for the BAC-P and BAC-Zn adsorbents were 0.8451 and 0.1266, respectively, which are not close to unity.

The kinetic plots for the intraparticle diffusion model for the BAC-P and BAC-Zn adsorbents in this study were linear with R^2 values of 0.9409 and 0.9194, respectively; unexpectedly, the derived plots did not go through the origin of the graph: intercepts, c, were observed and reported as shown in Table 5 and Figure 17. Therefore, since correlating the kinetic data with equation (13) gave a straight line, the interception, c, of these plot helps in the determination of the boundary layer thickness of the surface of the adsorbent. Therefore, the larger the intercept, the greater the boundary layer thickness, and the smaller the intercept, the lesser the boundary layer thickness and effect. With the IPD model, if the plots pass through the origin, it can then be concluded that the rate-determining step was the intraparticle diffusion, and hence it cannot be neglected in understanding the kinetic nature of the process. As shown in Figure 17, the kinetic plots of BAC-P and BAC-Zn adsorbents with intercepts of −0.0023 and −0.0072 $g\, g^{-1}$, respectively, indicated that the intraparticle diffusion was not the rate-limiting step in the sorption process of Cu(II) ions on the derived activated carbons with a small degree of boundary layer diffusion.

Also, Table 5 illustrates the kinetic parameters and the R^2 values for the Elovich kinetic model shown in Figure 18 and the Lagergren pseudo-first order kinetic model shown in Figure 15 for the adsorption process on the prepared adsorbents. Furthermore, the R^2 values were the highest for the former, i.e., Elovich model, with values for the BAC-P and BAC-Zn adsorbents as 0.9798 and 0.9682, respectively. The Lagergren pseudo-first-order kinetic model also indicated that R^2 values were somewhat high with the $q_{e,\,\exp\,t}$ and $q_{e,calc}$ of both the BAC-P and BAC-Zn adsorbents in great consonance. However, due to the fact that the coefficients of

Table 5: Kinetic model constants and coefficient of correlation values of different kinetic models for Cu(II) ions.

Kinetic models	Parameters	Adsorbents	
		BAC-P	BAC-Zn
Fractional power	$k_f * 10^3\,(\mathrm{mg\,g^{-1}})$	0.0253	0.0218
	$\nu\,(\mathrm{min^{-1}})$	0.0126	0.0163
	R^2	0.9090	0.8963
Pseudo-first order	$k_1\,(L\,\mathrm{min^{-1}})$	0.0132	0.0222
	$q_{e,\exp t} * 10^3\,(\mathrm{mg\,g^{-1}})$	0.0652	0.0728
	$q_{e,calc} * 10^3\,(\mathrm{mg\,g^{-1}})$	0.0658	0.1111
	R^2	0.9454	0.9329
Pseudo-second order	$k_2 * 10^{-6}\ (\mathrm{g\,mg^{-1}\,min^{-1}})$	0.5390	3.9200
	$h\ (\mathrm{mg\,g^{-1}\,min^{-1}})$	0.6475	0.4009
	$q_{e,\exp t} * 10^3\,(\mathrm{mg\,g^{-1}})$	0.0652	0.0728
	$q_{e,calc} * 10^3\,(\mathrm{mg\,g^{-1}})$	0.1096	0.3198
	R^2	0.8451	0.1266
Intraparticle diffusion	$k_{ip}\ (\mathrm{mg\,(g\,min)^{-0.5}})$	0.0335	0.0398
	c = intercept	−0.0023	−0.0072
	R^2	0.9409	0.9194
Elovich	$\beta_e * 10^{-2}\,(\mathrm{g\,mg^{-1}})$	4.7393	3.5590
	$a_e\,(\mathrm{mg\,g^{-1}})$	0.0351	0.0344
	$\alpha_e\,(\mathrm{mg\,g^{-1}\,min^{-1}})$	1.8567	1.5930
	R^2	0.9798	0.9682

determination for the derived activated carbons was outside of the 5% confidence limit, the Lagergren pseudo-first-order kinetic model was not considered to have fitted the kinetics data adequately. Therefore, from all indications, it can be corroborated that the kinetics data fitted exceedingly well with the Elovich kinetic model for the adsorbents investigated. Thus, the Elovich model can be considered the rate-limiting/determining step; however, due to the major limitation of its inability to analyze the slow-step kinetics in the adsorption process, the kinetics data were further investigated using the Boyd model [81]. The Boyd kinetics is given as follows:

$$F_B = 1 - \frac{6}{\pi^2}\exp\left(-B_t\right), \tag{16}$$

$$B_t = -In\left(1 - F_B\right) - 0.4977, \tag{17}$$

where F_B $(= q_t/q_e)$ is the fraction of solute adsorbed at a time t. The values of B_t was computed according to equation (16) for each value of F_B and then plotted against time to construct the Boyd plots [82]. The B_t values were plotted versus t, as indicated in Figure 19 for the BAC-P and BAC-Zn adsorbents. From Figure 19, the plots for each of the adsorbents were linear without passing through the origin, indicating that the adsorption of Cu(II) ions onto the chemically treated carbons was mainly governed by external mass transport (film diffusion) where the diffusion of the Cu^{2+} adsorbate molecules into the adsorbent particles was the slow step [30, 83].

3.2.5. Correlation of Equilibrium Adsorption Data of Cu(II) Ions. Adsorption equilibrium isotherm models describe how much of the adsorbate is adsorbed onto the adsorbent [84, 85]. The phenomenon is usually a function of the concentration of the adsorbates in an aqueous phase or pressure of the adsorbate in a gaseous phase at a constant temperature. The study of the equilibrium characteristics of the adsorbents used for this study includes the adsorption isotherms of Langmuir, Freundlich, Elovich, and Sips. The Langmuir isotherm model is generally based on the assumption of a homogenous adsorption process within the adsorbent surface with a uniformly distributed energy level [86]. It is characterized by the fact that once the adsorbate molecule is attached on a particular site, no further adsorption can take place, inferring a monolayer adsorption process. The model is given as

Table 6: Nature of the process depending on the value of the separation factor (R_L) [87].

$R_L > 1$	Unfavourable
$R_L = 1$	Linear
$0 < R_L < 1$	Favourable
$R_L = 0$	Irreversible

$$q_e = \frac{q_{\max} K_L c_e}{1 + K_L c_e}. \tag{18}$$

Equation (18) can be linearized as

$$\frac{1}{q_e} = \frac{1}{K_L q_{\max}}\frac{1}{c_e} + \frac{1}{q_{\max}}. \tag{19}$$

The importance of the Langmuir isotherm can be explained by a dimensionless constant, i.e., equilibrium parameter or separation factor, R_L, given by [51]:

$$R_L = \frac{1}{1 + K_L c_0}. \tag{20}$$

The separation factor R_L indicates the nature of the particular sorption uptake process as illustrated in Table 6.

Freundlich isotherm illustrates that adsorption processes are heterogeneous with the energy levels distributed

Table 7: Adsorption isotherm parameters for the adsorption of Cu(II) ions onto BAC-P and BAC-Zn adsorbents.

Langmuir					
BAC-P			BAC-Zn		
Error function	Parameters		Error function	Parameters	
$R^2 = 0.9555$	q_{max} (g g^{-1})	0.5889	$R^2 = 0.9742$	q_{max} (g g^{-1})	0.2251
	K_L (L g^{-1})	0.2040		K_L (L g^{-1})	1.2912
Freundlich					
$R^2 = 0.9460$	K_F (g g^{-1}) (L g^{-1})$^{1/n}$	0.0885	$R^2 = 0.9302$	K_F (g g^{-1}) (L g^{-1})$^{1/n}$	0.1919
	n(−)	1.1962		n(−)	1.1364
Elovich					
$R^2 = 0.3609$	K_E (L g^{-1})	1.0373	$R^2 = 0.0015$	K_E (L g^{-1})	0.0757
	q_{max} (g g^{-1})	0.1348		q_{max} (g g^{-1})	3.2154
Sips (Langmuir–Freundlich)					
$R^2 = 0.9529$	K_s (L g^{-1})	0.2144	$R^2 = 0.8846$	K_s (L g^{-1})	0.2837
	β_s (−)	1.1357		β_s (−)	1.0822
	a_s (L g^{-1})	2.4341		a_s (L g^{-1})	0.3329

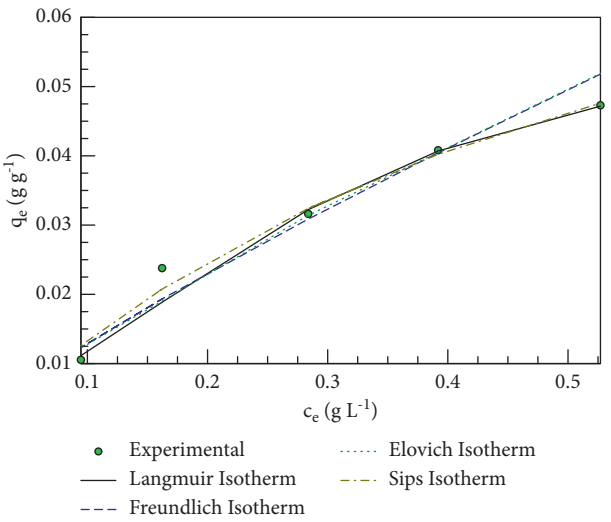

Figure 20: Adsorption isotherm models for Cu(II) ions adsorption onto the BAC-P adsorbent.

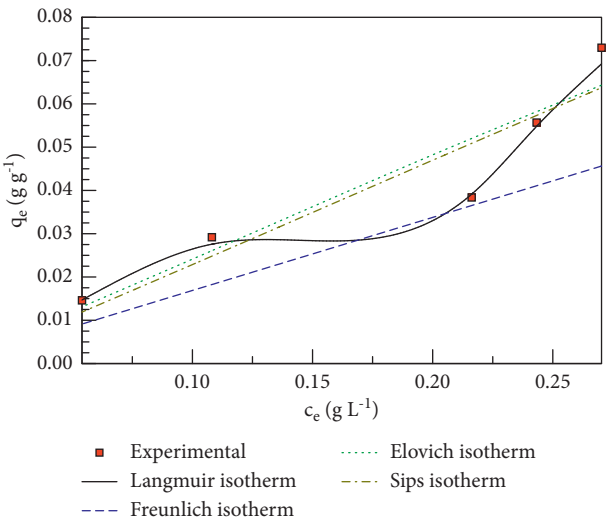

Figure 21: Adsorption isotherm models for Cu(II) ions adsorption onto the BAC-Zn adsorbent.

nonuniformly and also proposing reversible adsorption with a great probability of a multilayer adsorption process [88]. Equation (21) shows the Freundlich isotherm model:

$$q_e = K_F c_e^{1/n}, \tag{21}$$

whose linear form can be expressed as follows:

$$Inq_e = InK_F + \frac{1}{n} Inc_e, \tag{22}$$

where K_F is a measure of adsorption capacity and n is defined as the heterogeneity of the process.

The Elovich isotherm model is based on a kinetic principle assumption that the sites available for adsorption increase exponentially with respect to adsorption, which implies multilayer adsorption [89]. It is expressed by the following relation (equation (23)):

$$\frac{q_e}{q_{max}} = K_E c_e \exp\left(-\frac{q_e}{q_{max}}\right). \tag{23}$$

Table 8: Separation factors for the adsorption of Cu(II) ions onto the prepared adsorbents.

	Separation factor (R_L)	
c_0 (mg L^{-1})	BAC-P	BAC-Zn
200	0.9608	0.7949
400	0.9246	0.6596
600	0.8909	0.5637
800	0.8597	0.4921
1000	0.8306	0.4367

The Elovich isotherm model can be linearized as given in equation (24):

$$\ln\left(\frac{q_e}{c_e}\right) = \ln\left(q_{max} K_E\right) - \frac{q_e}{q_{max}}. \tag{24}$$

Sips isotherm is an evolved form of the combination of the Freundlich and Langmuir isotherms for the prediction of heterogeneous adsorption systems and thereby nullifying

Table 9: Comparison of the maximum monolayer adsorption capacity for Cu(II) ions onto various adsorbents.

Adsorbent	Parameter		$q_{max}\,(mg\,g^{-1})$	Reference
	pH	Temp. (K)		
Green vegetable waste	3.5	—	75.00	[44]
Hazelnut husks	6.7	291	6.645	[93]
Palm shell	3.0	—	18.60	[64]
Hazelnut shell	5.0	298	199.4	[94]
SP-sewage sludge	5.0	298	7.73	[95]
SZ-sewage sludge	5.0	298	10.56	[95]
Tunisian date stones	5.0	293	31.25	[96]
Rubberwood sawdust	5.7	303	5.72	[97]
Rice hulls	5.3	293	3.92	[98]
Treated *Tectona grandis*	7.0	300	87.00	[72]
Tectona grandis (Teak bark)	6.8	300	22.90	[72]
Defatted papaya seed	5.5	303	17.29	[99]
Nanocomposite adsorbent	5.2	298	173.62	[14]
BAC-P sugarcane bagasse	4.5	303	589	This work
BAC-Zn sugarcane bagasse	4.5	303	225	This work

BAC-P: H_3PO_4 activated sugarcane bagasse, BAC-Zn: $ZnCl_2$ activated sugarcane bagasse, SP: phosphatic, SZ: $ZnCl_2$.

the limitation associated with rising concentrations of particular adsorbates of the Freundlich isotherm model. The Sips isotherm model reduces to the Freundlich isotherm at low adsorbate concentrations while at high adsorbate concentrations, the isotherm predicts the adsorption capacity of an adsorbent in the form of the Langmuir isotherm with respect to monolayer adsorption [90]. The isotherm model is given mathematically as

$$q_e = \frac{K_s c_e^{\beta_s}}{1 + a_s c_e^{\beta_s}}. \tag{25}$$

The linear form of equation (25) is specified as

$$In(c_e) = -\frac{1}{\beta_s} In\left(\frac{K_s}{q_e}\right) + \frac{1}{\beta_s} In(a_s), \tag{26}$$

where K_s is defined as the Sips isotherm model constant (L/g), β_s is the Sips isotherm model exponent, and a_s is the Sips isotherm model constant (L/mg).

The coefficient of determination, R^2, was the benchmark used to certify the fitting of the equilibrium data to the different isotherm models as shown in Table 7, while the experimental equilibrium data with the corresponding fitted theoretical isotherms for the adsorption of Cu(II) ions onto the prepared adsorbents are shown in Figures 20 and 21. From the R^2 values, Langmuir isotherm was emphatically the best in correlation with the equilibrium adsorption data of Cu^{2+} ions removal from wastewater using BAC-P and BAC-Zn as adsorbents. The maximum adsorption uptake capacities for the Cu^{2+} ions were 589 and 225 $mg\,g^{-1}$ for BAC-P and BAC-Zn, respectively, at an ambient temperature of 30°C as stated in Table 7. These parameters were also used for the prediction of the nature and affinity of the Cu^{2+} ions toward the surfaces of the prepared adsorbents using the dimensionless separation factor R_L, as indicated in equation (20). The R_L values obtained were in the range $0 < R_L < 1$ (Table 8) for the Cu(II) ions concentration studied in this work ($200 \le c_0 \le 1000\,mgL^{-1}$) for both the prepared adsorbents. As indicated in Table 8, the R_L values obtained shows that the adsorption of Cu^{2+} ions onto the surface sites of BAC-P and BAC-Zn adsorbents was favourable as corroborated in previous studies [91, 92]. It can be observed from Figures 20 and 21 that the Langmuir isotherm model best fitted the equilibrium data of Cu^{2+} ion adsorption onto BAC-P and BAC-Zn adsorbents, especially when compared with Freundlich, Elovich, and Sips isotherm models. This is authenticated by the high values of R^2, compared with the other isotherm models. The comparison of the maximum monolayer adsorption capacity, q_{max}, of Cu^{2+} ions onto other various prepared adsorbents from literature is presented in Table 9.

The Freundlich isotherm model, as indicated in equation (21), showed a relatively high coefficient of determination with $n > 1$ for both BAC-P and BAC-Zn adsorbents (Table 7). The value of n in the Freundlich isotherm model gives a relative inference of the favourability of a sorption process. Generally, where $2 < n < 10$, the process is good; $1 < n < 2$, moderately difficult, and $n < 1$ shows poor sorption characteristics [30, 100]. The n values of the prepared adsorbents illustrate a moderately difficult sorption characteristic; hence, the Freundlich isotherm can somewhat be relatively used to correlate the adsorption data of Cu^{2+} ions removal using BAC-P and BAC-Zn as adsorbents.

The estimated values of the Elovich and Sips isotherm model parameters and their corresponding R^2 values are indicated in Table 7. From the R^2 values, the Elovich isotherm model was way off unity, while that of the Sips isotherm was in contrast, that is, close to unity but just short of that of the Langmuir model. This also shows the Sips isotherm model could represent the phenomenon of Cu^{2+} ions adsorption onto the two adsorbents studied.

3.2.6. Proposed Adsorption Mechanism of Cu(II) Ions onto BAC-P and BAC-Zn Adsorbents. The reaction mechanism of the adsorption of Cu^{2+} onto the BACs was proposed by noting the role of the carboxyl (-COOH) and hydroxyl (OH)

groups in the adsorption of Cu^{2+} on BACs by monitoring the pH during the adsorption process. The proposed adsorption mechanism is most likely dependent on the ion exchange between the surface of the BACs and Cu(II) metal ions, which have negatively and positively charged surface sites, respectively. Many other researchers have observed with keen interest, similar correlations between the metal ions adsorbed onto activated carbon and the released protons from the carboxyl group [101, 102]. From pH studies, it was observed that the adsorption of copper at very low-level pH occurs by ion exchange of $2H^+$ on the active sites on the surface of the BACs with a Cu^{2+} ion from solution; while at higher concentrations, other forms of ion exchange and surface complexation with oxygen ions occur at the active sites on the surface of the adsorbent. The reactions represented in equations (27) and (28) suggest that the Cu(II) ions uptake results from the formation of metal-complexes (unitary) during the adsorption process and the proposed adsorption mechanism:

$$S - COOH + Cu^{2+} \rightleftharpoons S - COO^{-}\,Cu^{2+} + H^{+}, \quad (27)$$

$$-C_n + 2H_2O \rightleftharpoons -C_nH_3O^{+} + OH^{-}, \quad (28)$$

where S-COOH signifies the carboxyl group on the surface of the BACs [103] and $-C_n$ represents the carbon layer probably controlling the adsorption mechanism being characterized by few surface acidic groups [102, 103].

4. Conclusions

From the study of the sorption properties of sugarcane bagasse activated carbon (BAC) under simulated contaminant conditions, this work has shown the feasibility of chemically activated BAC in the removal of copper(II) ions from industrial wastewater. Chemically treating the sugarcane bagasse using phosphoric acid (H_3PO_4) and zinc chloride ($ZnCl_2$), respectively, improved the overall specific surface area of the adsorbents, thereby increasing the adsorption capacity of these adsorbents for Cu(II) ions. Based on the study done, it was inferred that the amount of Cu(II) ions adsorbed depended on operational parameters such as contact time, initial ion concentration, pH, and adsorbent dosage. The Elovich kinetic model best predicted the experimental kinetics data with high correlations, while the adsorption mechanism was best predicted by the Langmuir isotherm model. The maximum monolayer sorption capacity of BAC-P and BAC-Zn for Cu(II) ions was determined to be 589 mg g^{-1} and 225 mg g^{-1}, respectively. The principal reason the BAC-P adsorbent had a better adsorption capacity than BAC-Zn is obtained from the analysis of the S_{BET} and the zeta potential of the activated carbons: BAC-P had an S_{BET} before adsorption and pH_{IEP} of 427 m^2/g and 3.70, while BAC-Zn had 282 m^2/g and 5.26, respectively. From these results, it can be observed that BAC-P has a significantly larger surface area than BAC-Zn and a lower pH_{IEP} in comparison with BAC-Zn, thereby giving BAC-P the ability to adsorb Cu(II) ions more efficiently and have a greater adsorption capacity than BAC-Zn, as corroborated by these works [15, 31, 63, 99]. Therefore, this work has substantiated the fact that sugarcane bagasse can be used as a renewable resource to produce derived activated carbons, which are potentially more cost-effective and exceedingly efficient for the sorption of metal ions.

Abbreviations

c: Intercept
c_0: Adsorbate initial/inlet concentration, g L^{-1}
c_e: The equilibrium concentration of the solute in the bulk solution, g L^{-1}
K_E: Elovich equilibrium constant, L g^{-1}
K_F: Freundlich isotherm constant, $mg^{1-(1/n)}$ $L^{1/n}g^{-1}$
K_L: Langmuir isotherm constant, L mg^{-1}
K_s: Sips isotherm model constant, L g^{-1}
k_1: The rate constant of pseudo-first-order sorption, min^{-1}
k_2: The rate constant of pseudo-second-order sorption, g $(g.min)^{-1}$
k_f: Fractional power kinetic model constant, mg g^{-1}
k_{ip}: Intraparticle diffusion rate constant, mg g^{-1}
m: Mass of adsorbent, mg
n: Adsorption intensity (heterogeneity factor)
q_e: Amount of solute adsorbed per unit weight of specific adsorbent at equilibrium, mg g^{-1}
q_{max}: Maximum adsorption capacity, mg g^{-1}
q_t: Amount of solute adsorbed at time t, mg g^{-1}
R^2: Coefficient of determination
S: Specific surface area, m^2 g^{-1}
V: Volume, L
α_e: Initial rate of adsorption
β_e: Elovich kinetic model constant, g g-^{1}
β_s: Sips isotherm model exponent
v: The exponent of the fractional power model
BAC: Sugarcane bagasse activated carbon
BAC-P: Phosphoric acid activated sugarcane bagasse carbon
BAC-Zn: Zinc chloride activated sugarcane bagasse carbon.

Data Availability

The data are available from the corresponding author upon request.

Additional Points

Sugarcane bagasse was converted to activated carbon using H_3PO_4 acid and $ZnCl_2$ salt. Monocomponent adsorption of Cu^{2+} ions in industrial wastewater was carried out successfully. The maximum adsorption capacities of both the adsorbents were obtained as 589 and 225 mg g^{-1}, respectively.

Conflicts of Interest

On behalf of all authors, the corresponding author states that there are no conflicts of interest.

Authors' Contributions

Temiloluwa E. Amoo: TEA contributed to the methodology and data curation, provided software, and wrote the original draft of the study. KOA contributed to the conceptualization and supervision, provided software, reviewed and edited, and performed validation of the study. OAA contributed to the supervision and review of the study. COO contributed to the study methodology.

Acknowledgments

The authors are grateful to the Covenant University for providing a conducive environment and adequate support for carrying out this research work.

References

[1] P. Versilind, W. Aarne, A. William, and D. Reinhart, *Solid Waste Engineering*, Brooks/Cole of Thomson Inc, Boston, MA, USA, 1 edition, 2002.

[2] S. Kaligorou, *Solar Engineering Processes and Systems*, Elsevier, Waltham MA, USA, 2 edition, 2014.

[3] A. Benedicta and P. Davar, "Waste to wealth potentials of municipal solid waste: a case study of Ga-East Municipal Assembly, Ghana," *African Journal of Environmental and Waste Management*, vol. 2, no. 1, pp. 113–121, 2014.

[4] C. M. Teboho, J. M. Mokgaostsa, E. M. Tshwafo, Z. L. Linda, M. T. Oriel, and P. S. Sandile, "Sugarcane bagasse and cellulose polymer composites," in *Sugarcane-Technology and Research*, D. O. Alexandre, Ed., pp. 225–240, IntechOpen, London, UK, 1 edition, 2018.

[5] S. S. Dhaliwal, H. S. Oberoi, S. K. Sandhu, D. Nanda, D. Kumar, and S. K. Uppal, "Enhanced ethanol production from sugarcane juice by galactose adaptation of a newly isolated thermotolerant strain of Pichia kudriavzevii," *Bioresource Technology*, vol. 102, no. 10, pp. 5968–5975, 2011.

[6] J. T. Rainey and G. Covey, "Pulp and paper production from sugarcane bagasse," in *Sugarcane-based Biofuels and Bioproducts*, I. O'Hara and S. Mundree, Eds., pp. 1–24, Wiley-Blackwell, Hoboken, NJ, USA, 1 edition, 2016.

[7] UN.FAO, *How Many Animals We Eat Each Year*, UN FAO, Rome, Italy, 2017.

[8] T. L. Bezerra and A. J. Ragauskas, "A review of sugarcane bagasse for second-generation bioethanol and biopower production," *Biofuels, Bioproducts and Biorefining*, vol. 10, no. 5, pp. 634–647, 2016.

[9] C. Faur-Brasquet, K. Kadirvelu, and P. Le Cloirec, "Removal of metal ions from aqueous solution by adsorption onto activated carbon cloths: adsorption competition with organic matter," *Carbon*, vol. 40, no. 13, pp. 2387–2392, 2002.

[10] B. Keita, B. Jimenez, and P. Drechsel, "Extent and implications of agricultural reuse of untreated, partially treated and diluted waste waters in developing countries," *CAB Reviews: Perspective in Agriculture, Veterinary Science, Nutrition and Natural Resources*, vol. 3, no. 58, pp. 1–15, 2013.

[11] P. Tchounwou, C. Newsome, J. Williams, and K. Glass, "Copper induced cytotoxicity and transcriptional activation of stress genes in human liver carcinoma cells," *Metal Ions in Biology and Medicine*, vol. 10, pp. 285–290, 2008.

[12] E. B. Ibitoye, I. H. Lokman, M. N. M. Hezmee, Y. M. Goh, A. B. Z. Zuki, and A. A. Jimoh, "Extraction and physicochemical characterization of chitin and chitosan isolated from house cricket," *Biomedical Materials*, vol. 13, pp. 25009–25012, 2018.

[13] G. Tchobanoglous, F. L. Burton, and H. D. Stenset, *Wastewater Engineering, Treatment and Reuse*, McGraw-Hill, New York, N, USA, 2003.

[14] M. R. Awual, G. E. Eldesoky, T. Yaita et al., "Schiff based ligand containing nano-composite adsorbent for optical copper(II) ions removal from aqueous solutions," *Chemical Engineering Journal*, vol. 279, pp. 639–647, 2015.

[15] J. Thilagan, S. Gopalakrishnan, and T. A. Kannadasan, "Comparative study on adsorption of copper (ii) ions in aqueous solution by; chitosan blended with cellulose and cross linked by formaldehyde, chitosan immobilised on red soil, chitosan reinforced by banana stem fibre," *International Journal of Advances in Engineering & Technology*, vol. 3, no. 1, pp. 35–60, 2013.

[16] K. Sandesh, R. Suresh Kumar, and P. E. Jagadeeshbabu, "Rapid removal of cobalt (II) from aqueous solution using cuttlefish bones; Equilibrium, kinetics, and thermodynamic study," *Asia-Pacific Journal of Chemical Engineering*, vol. 8, 2013.

[17] A. W. Adamson, "Physical chemistry of surfaces," *Journal of the Electrochemical Society*, vol. 124, 1977.

[18] R.-S. Juang and C.-H. Chiou, "Feasibility of the use of polymer-assisted membrane filtration for brackish water softening," *Journal of Membrane Science*, vol. 187, no. 1-2, pp. 119–127, 2001.

[19] B. Eikebrokk and T. Saltnes, "NOM removal from drinking water by chitosan coagulation and filtration through light-weight expanded clay aggregate filters," *Journal of Water Supply: Research & Technology - Aqua*, vol. 51, no. 6, pp. 323–332, 2002.

[20] S. Muthusaravanan, N. Sivarajasekar, J. S. Vivek et al., "Phytoremediation of heavy metals: mechanisms, methods and enhancements," *Environmental Chemistry Letters*, vol. 16, pp. 1339–1359, 2018.

[21] P. C. Vandevivere, R. Bianchi, and W. Verstraete, "Treatment and reuse of wastewater from the textile wet-processing industry: review of emerging technologies," *Journal of Chemical Society*, vol. 72, no. 4, pp. 289–302, 1998.

[22] M. Naushad, A. Mittal, M. Rathore, and V. Gupta, "Ion-exchange kinetic studies for Cd(II), Co(II), Cu(II), and Pb(II) metal ions over a composite cation exchanger," *Desalination and Water Treatment*, vol. 54, pp. 2883–2890, 2014.

[23] M. R. Awual, M. Ismael, T. Yaita et al., "Trace copper(II) ions detection and removal from water using novel ligand modified composite adsorbent," *Chemical Engineering Journal*, vol. 222, pp. 67–76, 2013.

[24] D. Moreno, R. Gómez, and L. Giraldo, "Removal of Mn, Fe, Ni and Cu ions from wastewater using cow bone charcoal," *Materials*, vol. 3, no. 1, pp. 452–466, 2010.

[25] W. C. Leung, M.-F. Wong, H. Chua, W. Lo, and P. H. F. Yu, "Removal and recovery of heavy metals by bacteria isolated from activated sludge treating industrial effluents and municipal wastewater," *Water Science and Technology*, vol. 41, pp. 233–240, 2000.

[26] O. A. Olafadehan, K. E. Abhulimen, A. I. Adeleke, C. V. Njoku, and K. O. Amoo, "Production and characterization of derived composite biosorbents from animal bone," *African Journal of Pure and Applied Chemistry*, vol. 13, no. 2, pp. 12–26, 2019.

[27] M. A. Barakat, "New trends in removing heavy metals from industrial wastewater," *Arabian Journal of Chemistry*, vol. 4, pp. 361–377, 2010.

[28] USEPA, *United States Environmental Protection Agency Priority Pollutant List 40 CFR Part 423 Appendix A*, USEPA, Washington, DC, USA, 2014.

[29] O. A. Ajayi and A. S. Olawale, "A comparative study of thermal and chemical activation of canarium schweinfurthii nutshell," *Journal of Applied Sciences Research*, vol. 5, no. 12, pp. 2148–2152, 2009.

[30] O. A. Olafadehan, O. Y. Akpo, O. Enemuo, K. O. Amoo, and O. G. Abatan, "Equilibrium, kinetic and thermodynamic studies of biosorption of zinc ions from industrial wastewater using derived composite biosorbents from walnut shell," *African Journal of Environmental Science and Technology*, vol. 12, no. 9, pp. 335–356, 2018.

[31] T. V. Thuan, P. V. Thind, B. T. Quynh et al., "Production of Activated Carbon from sugarcane bagasse by chemical activation with ZnCl2; Preparation and characterization study," *Research Journal of Chemical Sciences*, vol. 6, no. 5, pp. 42–47, 2016.

[32] APHA, *Standard Methods for the Examination of Water and Wastewater*, APHA, Washington, DC, USA, 17 edition, 1989.

[33] R. P. Jeyakumar and V. Chandrasekaran, "Adsorption of Lead (II) ions by activated carbons prepared from marine green algae: equilibrium and kinetics studies," *International Journal of Integrated Care*, vol. 5, no. 2, 2014.

[34] G. G. Stavropoulos, P. Samaras, and G. P. Sakellaropoulos, "Effect of activated carbons modification on porosity, surface structure and phenol adsorption," *Journal of Hazardous Materials*, vol. 151, pp. 414–421, 2008.

[35] A. S. Alzaydian, "Adsorption of methylene blue from aqueous solution onto a low-cost natural Jordanian Tripoli," *American Journal of Applied Sciences*, vol. 6, no. 6, pp. 1047–1058, 2009.

[36] ASTM-D-4607(2006), *Standard Test Method for Determination of Iodine Number of Activated Carbon*, American Society for Testing and Materials (ASTM) International, West Conshohocken, PA, USA, 1994.

[37] A. Beer, "Bestimmung der absorption des rothen lichts in farbien flussigkeiten," *Annalen Der Physik*, vol. 86, pp. 74–88, 1852.

[38] P. N. Cheremisinoff and F. Ellerbusch, *Carbon Adsorption Handbook*, Ann Arbor Science, Ann Arbor, MI, USA, 1 edition, 1978.

[39] S. Dash, H. Chaudhuri, G. Udayabhanu, and A. Sarkar, "Fabrication of inexpensive polyethylenimine-functionalized fly ash for highly enhanced adsorption of both cationic and anionic toxic dyes from water," *Energy & Fuels*, vol. 30, no. 8, pp. 6646–6653, 2016.

[40] C. Tang, Y. Shu, R. Zhang et al., "Comparison of the removal and adsorption mechanisms of cadmium and lead from aqueous solution by activated carbons prepared from Typha angustifolia and Salix matsudana," *Royal Society of Chemistry Advances*, vol. 7, pp. 16092–16103, 2017.

[41] H. Demiral and İ. Demiral, "Surface properties of activated carbon prepared from wastes," *Surface and Interface Analysis*, vol. 40, no. 3-4, pp. 612–615, 2008.

[42] E. Demirbas, "Adsorption of cobalt (II) ions from aqueous solution onto activated carbon prepared from hazelnut shells," *Adsorption Science and Technology*, vol. 21, pp. 951–963, 2003.

[43] S. Vilvanathan and S. Shanthakumar, "Biosorption of Co(II) ions from aqueous solution using Chrysanthemum indicum: kinetics, equilibrium and thermodynamics," *Process Safety and Environmental Protection*, vol. 96, 2015.

[44] M. I. Sabela, K. Kunene, S. Kanchi et al., "Removal of copper (II) from wastewater using green vegetable waste derived activated carbon: an approach to equilibrium and kinetic study," *Arabian Journal of Chemistry*, vol. 12, pp. 4331–4339, 2019.

[45] J. Villarroel-Rocha, D. Barrera, J. J. Arroyo-Gomez, and K. Sapag, "Insights of adsorption isotherms with different gases at 77 K and their use to assess the BET area of nanoporous silica materials," *Adsorption*, vol. 27, pp. 1081–1093, 2021.

[46] M. Tsezos and J. P. Bell, "Comparison of the biosorption and desorption of hazardous organic pollutants by live and dead biomass," *Water Research*, vol. 23, pp. 561–568, 1989.

[47] T. F. Lin and J. K. Wu, "Adsorption of arsenite and arsenate within activated alumina grains: equilibrium and kinetics," *Water Research*, vol. 35, pp. 2049–2057, 2001.

[48] A. A. Khan, M. Muthukrishnan, and B. K. Guha, "Sorption and transport modeling of hexavalent chromium on soil media," *Journal of Hazardous Materials*, vol. 54, pp. 444–454, 2009.

[49] K. O. Amoo, O. A. Olafadehan, and T. O. Ajayi, "Optimization studies of chitin and chitosan production from Penaeus notialis shell waste," *African Journal of Biotechnology*, vol. 18, no. 27, pp. 670–688, 2019.

[50] P. H. F. Pereira, H. C. J. Voorwald, M. O. H. Cioffi, D. R. Mulinari, S. M. D. Luz, and M. L. C. Da Silva, "Sugarcane bagasse pulping and bleaching: thermal and chemical characterization," *Bioresources*, vol. 6, no. 3, pp. 2471–2482, 2011.

[51] C. R. Girish and V. Ramachandra Murty, "Adsorption of phenol from aqueous solution using Lantana camara, forest Waste: kinetics, isotherm, and thermodynamic studies," *International Scholarly Research Notices*, vol. 2014, Article ID 201626, 13 pages, 2014.

[52] H. B. Senturk, D. Ozdes, A. Gundogdu, C. Duran, and M. Soylak, "Removal of phenol from aqueous solutions by adsorption onto organomodified Tirebolu bentonite: equilibrium, kinetic and thermodynamic study," *Journal of Hazardous Materials*, vol. 172, no. 1, pp. 353–362, 2009.

[53] J. P. Kushwaha, V. C. Srivastava, and I. D. Mall, "Treatment of dairy wastewater by commercial activated carbon and bagasse fly ash: parametric, kinetic and equilibrium modelling, disposal studies," *Bioresource Technology*, vol. 101, no. 10, pp. 3474–3483, 2010.

[54] I. A. W. Tan, A. L. Ahmad, and B. H. Hameed, "Preparation of activated carbon from coconut husk: optimization study on removal of 2,4,6-trichlorophenol using response surface methodology," *Journal of Hazardous Materials*, vol. 153, no. 1–2, pp. 709–717, 2008.

[55] R. T. Morrison and R. N. Boyd, *Organic Chemistry*, Pearson Education, London, UK, 2004.

[56] C. Namasivayamand and D. Kavitha, "IR, XRD and SEM-studies on the mechanism of adsorption of dyes and phenols by coir pith carbon from aqueous phase," *Microchemical Journal*, vol. 82, no. 1, pp. 43–48, 2006.

[57] A. T. Mohd Din, B. H. Hameed, and A. L. Ahmad, "Batch adsorption of phenol onto physiochemical-activated coconut shell," *Journal of Hazardous Materials*, vol. 161, no. 2–3, pp. 1522–1529, 2009.

[58] K. P. Singh, A. Malik, S. Sinha, and P. Ojha, "Liquid-phase adsorption of phenols using activated carbons derived from agricultural waste material," *Journal of Hazardous Materials*, vol. 150, no. 3, pp. 626–641, 2008.

[59] S. Ferraris, M. Cazzola, V. Peretti, B. Stella, and S. Spriano, "Zeta Potential measurements on solid surfaces for in vitro biomaterials testing: surface charge, reactivity upon contact with fluids and protein absorption," *Frontiers in Bioengineering and Biotechnology*, vol. 6, no. 60, pp. 60–67, 2018.

[60] P. Novak and V. Havlicek, "Protein extraction and precipitation," in *Proteomic Profiling and Analytical Chemistry: The Crossroads*, P. Ciborowski and J. Silberring, Eds., pp. 51–62, Elsevier, Amsterdam, Netherlands, 2 edition, 2016.

[61] S. Bhattacharjee, "DLS and zeta potential - what they are and what they are not?" *Journal of Controlled Release*, vol. 235, pp. 337–351, 2016.

[62] K. O. Amoo, E. N. Onyeozili, E. E. Kalu, J. A. Omoleye, and V. E. Efeovbokhan, "Activity of varying compositions of Co-Ni-P catalysts for the methanolysis of ammonia borane," *International Journal of Hydrogen Energy*, vol. 41, no. 46, pp. 21221–21235, 2016.

[63] M. El-Azazy, I. Nabil, S. S. Hassan, and A. S. El-Shafie, "Adsorption characteristics of pristine and magnetic biochar with resoect to clofazimine," *Nanomaterials*, vol. 11, no. 963, pp. 1–24, 2021.

[64] G. Issabayeva, M. K. Aroua, and N. M. Sulaiman, "Study on palm shell activated carbon adsorption capacity to remove copper ions from aqueous solutions," *Desalination*, vol. 262, no. 1–3, pp. 94–98, 2010.

[65] A. Saeed, M. W. Akhter, and M. Iqbal, "Removal and recovery of heavy metals from aqueous solution using papaya wood as a new biosorbent," *Separation and Purification Technology*, vol. 45, 2005.

[66] J. Ma, F. Yu, L. Zhou et al., "Enhanced adsorptive removal of methyl orange and methylene blue from aqueous solution by alkali-activated multiwalled carbon nanotubes," *ACS Applied Materials and Interfaces*, vol. 4, pp. 5749–5760, 2012.

[67] Y. Jiang, H. Pang, and B. Liao, "Removal of copper(II) ions from aqueous solution by modified bagasse," *Journal of Hazardous Materials*, vol. 164, 2009.

[68] P. N. Sudha, S. Aisverya, T. Gomathi et al., "Application of chitin/chitosan and its derivatives as adsorbents, coagulants, and flocculants," in *Chitosan*, pp. 453–487, Scrivener Publishing LLC, Beverly, MA, USA, 2017.

[69] N. Tumin, A. Chua, Z. Zawani, and S. Rashid, "Adsorption of copper from aqueous solution by Elais guineensis kernel activated carbon," *Journal of Engineering Science & Technology*, vol. 3, no. 3, pp. 180–189, 2008.

[70] K. Y. Foo and B. H. Lee, "Preparation of activated carbon from sugarcane bagasse by microwave assisted activation for the remediation of semi-aerobic landfill leachate," *Bioresource Technology*, vol. 134, pp. 166–172, 2013.

[71] O. Abdelwahab, "Kinetic and isotherm studies of copper (II) removal from wastewater using various adsorbents," *Egyptian Journal of Aquatic Research*, vol. 33, no. 1, pp. 125–143, 2007.

[72] C. J. Ajaelu, L. Ibironke, and A. B. Oladinni, "Copper (II) ions adsorption by untreated and chemically modified Tectona grandis (Teak bark): kinetics, equlibrium and thermodynamic studies," *African Journal of Biotechnology*, vol. 18, no. 14, pp. 296–306, 2019.

[73] J. Zeldowitsch, "Uber den mechanismus der katalytischen oxydation von CO an MnO2," *Acta Physicochim. URSS*, vol. 1, pp. 364–449, 1934.

[74] T. Albrecht, J. Addai-Mensah, and D. Fornasiero, "Effect of pH, concentration and temperature on copper and zinc hydroxide formation/precipitation in solution," *Engineering a Better World*, pp. 1–10, Institution of Engineers, 2011.

[75] G. B. Baes and R. E. Mesmer, *Hydrolysis of Cations*, John Wiley and Sons, Hoboken, NJ, USA, 1976.

[76] A. A. Okoya, A. B. Akinyele, O. S. Amuda, and I. E. Ofoezie, "Chitosan-grafted carbon for the sequestration of heavy metals in aqueous solution," *American Chemical Science Journal*, vol. 11, no. 3, pp. 1–14, 2016.

[77] J. C. Y. Ng, W. H. Cheung, and G. McKay, "Equilibrium studies for the sorption of lead from effluents using chitosan," *Chemosphere*, vol. 52, pp. 1021–1030, 2003.

[78] S. Lagergren, "About the theory of so-called adsorption of soluble substances," *Kungliga Svenska Vetenskapsakademiens*, vol. 24, no. 4, pp. 1–39, 1898.

[79] J. Walter Weber and J. Carrell Morris, "Kinetics of adsorption on carbon from solution," *Journal of the Sanitary Engineering Division*, vol. 89, 1963.

[80] S. Yakout and E. Elsherif, "Batch kinetics, isotherm and thermodynamic studies of adsorption of strontium from aqueous solutions onto low cost rice-straw based carbons," *Carbon-Science and Technology*, vol. 1, pp. 144–153, 2010.

[81] G. E. Boyd, A. W. Adamson, and L. S. Myers Jr, "The exchange adsorption of ions from aqueous solutions by organic zeolites. II. Kinetics1," *Journal of the American Chemical Society*, vol. 69, no. 11, pp. 2836–2848, 1947.

[82] Y. S. Ho, J. F. Porter, and G. McKay, "Equilibrium isotherm studies for the sorption of divalent metal ions onto peat: copper, nickel and lead single component systems," *Water, Air, and Soil Pollution*, vol. 141, no. 1/4, pp. 1–33, 2002.

[83] S. Wang, H. M. Ang, and M. O. Tade, "Novel applications of red mud as coagulant, adsorbent and catalyst for environmentally benign processes," *Chemosphere*, vol. 72, no. 11, pp. 1621–1635, 2008.

[84] A. reza Rahmani, E. Hossieni, and A. Poormohammadi, "Removal of chromium (VI) from aqueous solution using electro-fenton process," *Environmental Processes*, vol. 2, no. 2, pp. 419–428, 2015.

[85] Z. Xu, J. Cai, and B. Pan, "Mathematical modeling fixed-bed adsorption in aqueous systems," *Journal of Zhejiang University-Science*, vol. 14, pp. 155–176, 2013.

[86] I. Langmuir, "The constitution and fundamental properties of solids and liquids. Part I. Solids," *Journal of the American Chemical Society*, vol. 38, no. 11, pp. 2221–2295, 1916.

[87] T. W. Webber and R. K. Chakkravorti, "Pore and solid diffusion models for fixed-bed adsorbers," *American Institute of Chemical Engineering Journal*, vol. 20, pp. 228–238, 1974.

[88] H. M. F. Freundlich, "Over the adsorption in solution," *The Journal of Physical Chemistry*, vol. 57, pp. 385–471, 1906.

[89] S. Y. Elovich and O. G. Larionov, "Theory of adsorption from nonelectrolyte solutions on solid adsorbents-2," *Experimental Verification of the Equation for the Adsorption Isotherm from Solutions*, Bulletin of the Academy of Sciences of the USSR Division of Chemical Science, Moscow, Russia, 1962.

[90] R. Sips, "Combined form of Langmuir and Freundlich equations," *The Journal of Chemical Physics*, vol. 16, pp. 490–495, 1948.

[91] R. Dabbagh, Z. Ashtiani Moghaddam, and H. Ghafourian, "Removal of cobalt(II) ion from water by adsorption using intact and modified Ficus carica leaves as low-cost natural sorbent," *Desalination and Water Treatment*, vol. 57, 2016.

[92] E. S. Z. El-Ashtoukhy, N. K. Amin, and O. Abdelwahab, "Removal of lead (II) and copper (II) from aqueous solution using pomegranate peel as a new adsorbent," *Desalination*, vol. 223, 2008.

[93] M. Imamoglu and O. Tekir, "Removal of copper (II) and lead (II) ions from aqueous solutions by adsorption on activated carbon from a new precursor hazelnut husks," *Desalination*, vol. 228, no. 1–3, pp. 108–113, 2008.

[94] D. D. Milenkovic, P. V. Dasic, and V. B. Veljkovic, "Ultrasound-assisted adsorption of copper (II) ions on hazelnut shell activated carbon," *Ultrasonics Sonochemistry*, vol. 16, pp. 557–563, 2009.

[95] X. Wang, X. Liang, Y. Wang et al., "Adsorption of copper (II) onto activated carbons from sewage sludge by microwave-induced phosphoric acid and zinc chloride activation," *Desalination*, vol. 278, pp. 231–237, 2011.

[96] F. Bouhamed, Z. Elouear, and J. Bouzid, "Adsorptive removal of copper(II) from aqueous solutions on activated carbon prepared from Tunisian date stones: equilibrium, kinetics and thermodynamics," *Journal of the Taiwan Institute of Chemical Engineers*, vol. 43, no. 5, pp. 741–749, 2012.

[97] M. H. Kalavathy, T. Karthikeyan, S. Rajgopal, and L. R. Miranda, "Kinetic and isotherm studies of Cu(II) adsorption onto H3PO4-activated rubber wood sawdust," *Journal of Colloid and Interface Science*, vol. 292, no. 2, pp. 354–362, 2005.

[98] T. Murat, I. Mustafa, and S. Omer, "Adsorption of copper and cadmium ions by activated carbon from Rice Hulls," *Turkish Jounal of Chemistry*, vol. 23, pp. 185–192, 1999.

[99] Z. N. Garba, I. Bello, A. Galadima, and A. Y. Lawal, "Optimization of adsorption conditons using central composite design for the removal of copper (II) and lead (II) by defatted papaya seed," *Karbala International Journal of Modern Science*, vol. 2, pp. 1–9, 2015.

[100] H. Chen, J. Zhao, G. Dai, J. Wu, and H. Yan, "Adsorption characteristics of Pb (II) from aqueous solution onto a natural biosorbent fallen Cinnamomoum Camphora leaves," *Desalination*, vol. 262, no. 1–3, pp. 151–157, 2010.

[101] M. O. Corapcioglu and C. P. Huang, "The adsorption of heavy metals onto hydrous activated carbon," *Water Research*, vol. 21, no. 9, pp. 1031–1044, 1987.

[102] S. A. Dastgheib and D. A. Rockstraw, "Pecan shell activated carbon: synthesis, characterization, and application for the removal of copper from aqueous solution," *Carbon*, vol. 39, no. 12, pp. 1849–1855, 2001.

[103] J. P. Mesquita, P. B. Martelli, and H. F. Gorgulho, "Characterization of copper adsorption on oxidized activated carbon," *Journal of the Brazilian Chemical Society*, vol. 17, no. 6, pp. 1133–1143, 2006.